Acetophenone hydrogenation and consecutive hydrogenolysis with Pd/CNT catalysts: Highlighting the synergy between single atoms and nanoparticles by kinetic modeling

Vincent Bernardin, Laurent Vanoye, Camila Rivera-Cárcamo, Philippe Serp, Alain Favre-Réguillon, Régis Philippe

Acetophenone hydrogenation and consecutive hydrogenolysis with Pd/CNT catalysts: highlighting the synergy between single atoms and nanoparticles by kinetic modeling

Vincent Bernardin,[1] Laurent Vanoye,[1] Camila Rivera-Cárcamo,[2] Philippe Serp,[2*] Alain Favre-Réguillon[1,3*], Régis Philippe[1*]

[1]Catalyse Polymérisation Procédés & Matériaux (CP2M), Université Lyon, UMR 5128 CNRS – CPE Lyon – UCBL, 43 boulevard du 11 novembre 1918, F-69100 Villeurbanne (France).

E-mail: regis.philippe@lgpc.cpe.fr

[2]ENSIACET, Université de Toulouse, LCC CNRS-UPR 8241, F-31030 Toulouse, (France).

E-mail : philippe.serp@ensiacet.fr

[3]Département Chimie-Vivant-Santé, Conservatoire National des Arts et Métiers, 292 rue Saint Martin, F-75003 Paris, (France).

E-mail: favrereg@cnam.fr

ABSTRACT

Understanding the cooperative action of palladium nanoparticles (NP) and palladium single atoms (SA) supported on carbon nanotubes (CNT) is essential for developing more efficient supported transition metal catalysts. In this work, the comparison of a series of Pd-catalysts on CNT having the same palladium loading (~1.4 wt%) but involving different and controlled SA/NP ratios (between 2 and 200) is described. The hydrogenation of acetophenone into 1-phenylethanol and its consecutive hydrogenolysis to ethylbenzene are the chosen test reactions. Appropriate kinetic modeling of these two consecutive reactions was performed and allowed a quantitative assessment of the activity differences between catalysts as well as the demonstration of a synergy between the two palladium species (SA and NP). The maximum activity was clearly dependent on the distribution of the surface palladium between SA and NP, and interestingly, different optima for the two reactions are evidenced. This work may offer a new perspective for the design and synthesis of supported transition metal catalysts with targeted catalytic performance.

Keywords: Palladium single atom catalyst; Palladium nanoparticles; Carbon nanotubes; Acetophenone; Kinetic modeling; Hydrogen

1. Introduction

The catalytic hydrogenation of organic compounds containing a carbonyl group is important in the synthesis of fine chemicals, pharmaceuticals, dyes, and agrochemicals. Acetophenone (AP) is a model molecule for evaluating and comparing supported catalysts for such a reaction. So far, catalytic systems such as Ni [1-3], Cu [4], Rh [5,6], and Pt [7-9] have been successfully used in the hydrogenation of acetophenone, but supported Pd catalysts are commonly used in the reduction of AP [2,10-19]. Pd promotes the formation of 1-phenylethanol (PE) and ethylbenzene (EB) in two consecutive reactions (Fig. 1) [13,20,21].

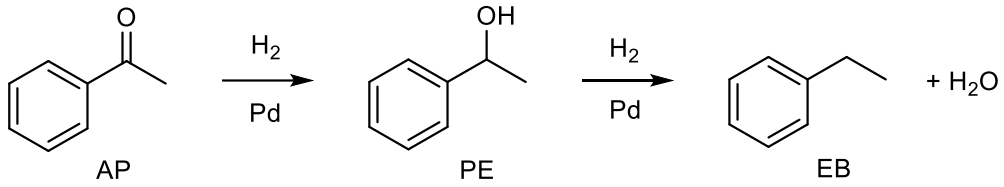

Fig. 1. Consecutive reactions steps involved in acetophenone hydrogenation and hydrogenolysis with Pd catalysts.

However, there are two problems related to the use of Pd. The first one is related to the lack of selectivity of the reaction, particularly related to the competition between the reduction and the hydrogenolysis steps. The second is related to the cost and the poor utilization of palladium in heterogeneous catalysts, which thus drives the search for alternatives. Recently, Pd single-atom (SA) catalysts have exhibited maximized atomic efficiency compared with conventional supported Pd nanoparticles (NP) catalysts due to 100 % metal dispersion and the presence of a single type of metal site [22]. SA catalysis demonstrated distinguishing performances [23], like CO oxidation [24], water gas shift reaction [25], hydroformylation [26], and electrocatalysis [27]. However, in the hydrogenation process [28], SA catalysts empower selectivity but at the expense of activity [29,30]. For instance, the specific properties of SA found valuable application in the selective hydrogenation of acetylene into ethylene [31-33] or 1,3-butadiene into butenes [34,35]. In contrast, the activities observed on double bonds, ketones, and even aldehydes are deceiving. This could be explained by the kinetically demanding dissociative pathway of H_2 on SA [36,37,38], especially if the substrate pre-coordinated SA sites [39].

Therefore, the improvement of the hydrogenation activity of Pd SA while maintaining its valuable properties has been addressed by different strategies. The first was to shorten the distance between SA so that two neighbouring SA provide adjacent active sites [39]. The properties of SA will be maintained while providing higher activity. The drawbacks of such a strategy are the large-scale preparation difficulties and the deactivation of atomically dispersed catalysts by sintering.

The second strategy was to use cooperativity between Pd SA and Pd NP [37,40-42]. H_2 dissociation is favoured on Pd NP compared to Pd SA, and hydrogen spillover on the support will enable the formation of the active H-Pd SA species [17,43-45]. We have reported a synthesis procedure of Pd catalysts supported on nano-structured carbon that allows controlling the SA/NP ratio [36,45]. These catalysts were demonstrated to be stable and highly active for alkenes hydrogenation [47,48].

The catalytic activities of these catalysts should depend on the combination of SA and NP [36], and the catalytic activities can be optimized by controlling such ratio. Herein, aiming to gain further insight into cooperativity between SA and NP, the performance of supported Pd on carbon nanotubes with different and controlled SA/NP ratio was studied for the hydrogenation/hydrogenolysis of acetophenone.

2. Experimental section

2.1. Catalysts and catalysts preparation

Pd_{Escat} (Strem chemicals, Product number Escat 1431) was used directly without further treatment. Pd_2 catalyst has been prepared using a classical wet impregnation method to obtain a high proportion of nanoparticles. The desired amount of palladium (II) nitrate dihydrate ($Pd(NO_3)_2.2H_2O$) (Sigma-Aldrich) was added to acetone (100 mL) containing 1 g of carbon nanomaterial to introduce 2 wt% of metal phase. The solution was sonicated at room temperature for 1 h and magnetically stirred overnight. The solution was then filtered and washed with acetone. The resulting solid was dried at 120 °C overnight. Finally, the Pd_2 catalyst was reduced in a horizontal furnace under a N_2/H_2 flow (20 vol% H_2) at 300 °C for 2 h (25°C to 300 °C at 10 °C/min).

Pd_{10}, Pd_{40}, Pd_{60}, and Pd_{200} catalysts have been prepared according to the procedure of P. Serp et al [36]. It consists of i) creating carboxylic groups on the support by nitric acid oxidation (step I), ii) decomposing these groups under an inert atmosphere to produce CO_2, some H_2 and carbon vacancies in the outer carbon nanotube layers (step II) and iii) depositing the metal on this defective and very reactive support (step III). For a given metal loading, if step III is performed once, mainly Pd SA are obtained; if it is performed several times (adjusting the amount of metal in each deposition), mixtures of SA and NP are obtained. The number of times that step III is performed for a given total metal loading modify the SA/NP ratio by increasing the relative number of NP. Bis (2-methylallyl)palladium precursor (Nanomeps) is used to perform these specific preparations. Its addition to the highly reactive activated CNT support containing the vacancies is done under an argon atmosphere and using an anhydrous pentane suspension of the support. At the end of each impregnation cycle, the precursor was decomposed under a N_2/H_2 flow (20 vol% H_2) at 80 °C for 1 h.

2.2. Catalysts characterization

The palladium content in the catalysts was determined by inductively coupled plasma optical emission spectroscopy (ICP-OES) performed at the LCC with a Thermo Scientific ICAP 6300 instrument. TEM and HR-TEM analyses were performed at the "Centre de microcaracterisation Raimond Castaing, UMS 3623, Toulouse" using a JEOL JEM 1011 CX-T electron microscope operating at 100 kV with a point resolution of 4.5 Å and a JEOL JEM 1400 electron microscope operating at 120 kV. The high-resolution analyses were conducted using a JEOL JEM 2100F equipped with a field emission gun (FEG) operating at 200 kV with a point resolution of 2.3 Å and a JEOL JEM-ARM200F Cold FEG operating at 200 kV with a point resolution of > 1.9 Å.

The particle size distribution was determined through several micrographs from different areas of the TEM grid (at least 300 particles). The size distributions reported as Pd atomic percentage (based on total atoms) in each size range were obtained by calculating the number of atoms (N) in each NP, assuming a spherical shape using an equation described in the literature [49]. The SA/NP ratio (a

number ratio) was measured from the STEM-HAADF analyses of at least 500 elements. Metal dispersion was evaluated from the fraction of SA and a universal mathematical relation between the mean relative size of metallic crystallites and their dispersion [50]. The samples were analysed by X-ray photoelectron spectroscopy (XPS) using a VG Escalab MKII spectrophotometer operating with a non-monochromatized Mg K source (1253.6 eV).

2.3. Reactivity measurements

Acetophenone catalytic hydrogenation was performed in a stirred tank reactor of 200 mL from Top Industrie. This reactor has 4 baffles and a gas-inducing Rushton turbine with 6 straight blades for efficient G-L-S contacting. Temperature control is provided by an electric shell (for heating) and a Ranque-Hilsch vortex device (for cooling). Typical catalytic tests were operated at 1200 rpm and 60 °C with 60 mg of Pd/CNT catalyst under an H_2 atmosphere at a constant pressure of 5 bar. The liquid phase consists of 120 mL of a 0.2 M acetophenone (Acros organics, 98%) solution in ethanol (VWR, absolute) previously purified by absorption on activated carbon. The reactor is thus operated in batch mode for the liquid and solid phases and in semi-batch mode for the gas because hydrogen was constantly fed via a pressure regulator and supplied by a calibrated and monitored reserve. Aliquots could be taken from the liquid phase and analyzed by GC-FID equipped with DB-1 and DB-WAX columns. The liquid phase temperature, the pressure inside the reactor, and the pressure and temperature of the reserve were acquired and recorded using Labview® at 1 Hz.

2.4. Kinetic and reactor modeling

Kinetic modeling studies were performed using Matlab® software (Matlab R2020b). A classical pseudo-homogeneous isothermal and isobaric stirred tank model has been used to simulate the liquid phase composition. The absence of physical limitations (G-L, L-S, and internal) has been verified thanks to classical chemical reaction engineering criteria and measurements (see supporting information). The Matlab routine is based on a Levenberg-Marquardt optimization algorithm and a Runge-Kutta solver. For the Pd_{Escat} catalyst, 6 kinetic parameters were adjusted and found significant and not correlated. For the comparison of the different catalysts, 4 kinetic constants were adjusted ($k_{hydrogenation}$, $k_{hydrogenolysis}$, K_{PE}, and K_{EB}+K_{H2O}), assuming the remaining adsorption parameters identical to the Pd_{Escat} reference catalyst. The objective function (OF) cleverly considers the complementary liquid composition and H_2 reserve consumption profiles with equal weight (see equation 1 below).

$$OF = \left\{\sum_i \sum_j \sum_k \left(\frac{C_{i,j,k}^{L,theo} - C_{i,j,k}^{L,exp}}{C_{ref}}\right)^2\right\} + \left\{\sum_l \frac{\overline{N_L}}{N_{G,l}} \sum_m \left(\frac{n_{l,m}^{G,theo} - n_{l,m}^{G,exp}}{V_L \cdot C_{AP,l,0}^L}\right)^2\right\} \quad (1)$$

In this equation, the first bracket refers to the liquid profiles involving "i" species in "j" experiments with "k" samplings. The second bracket corresponds to the H_2 consumption in "l" experiments with "m" data.

C_{ref} is a reference concentration of 0.2 mol/L; $\overline{N_L}$ is the average number of liquid sampling points for a single experiment; $N_{G,l}$ is the number of recorded pressure points in the experiment "l"; $C_{AP,l,0}^L$ is the initial AP concentration in the experiment "l". "L", "G", "theo", and "exp" superscripts refer to the liquid phase, the gas phase, theoretical and experimental values, respectively.

3. Results and Discussion

3.1. Synthesis and characterization

A series of Pd catalysts supported on carbon nanotubes were prepared by the method developed by P. Serp *et al* [36, 46]. The detailed characterization of the catalyst has been presented elsewhere [36], and Table 1**Erreur ! Source du renvoi introuvable.** summarizes the main characteristics of this series of catalysts conducted by STEM and XPS analyses. The Pd loading was set to ~1.4 wt% and the SA/NP ratio was varied from 10 to 200. This number ratio is recalled in the name of the catalyst. A commercial Pd/C catalyst (Pd_{Escat}) and a Pd/CNT catalyst containing mostly NP (Pd_2) have been taken as references for comparison.

Table 1.

Main characteristics of the investigated catalysts

Catalyst	Pd loading (wt%)	Average NP size[a)] (nm)	SA/NP ratio[b) c)] (-)	Pd in SA[c) d)] (atomic %)	Pd in NP surface[c) d)] (atomic %)	Pd in NP core[c) d)] (atomic %)	Dispersion[c) d)] (atomic %)	Pd^0 fraction[e)] (atomic %)	$Pd^{\delta+}$ fraction[e)] (atomic %)	$Pd^{\delta+}/Pd^0$ ratio[e)] (-)
Pd_2	2.04	2.2 ± 1.1	2	2	48	50	49	n.d.	n.d.	-
Pd_{10}	1.29	1.1 ± 0.6	10	17	74	9	89	41.8	58.2	1.4
Pd_{40}	1.43	0.9 ± 0.3	40	58	40[f)]	2[f)]	>95[f)]	22.0	78.0	3.5
Pd_{60}	1.37	0.8 ± 0.3	60	78	21[f)]	1[f)]	>95[f)]	15.2	84.7	5.5
Pd_{200}	1.33	0.5 ± 0.1	200	97	3[f)]	0[f)]	>95[f)]	14.2	85.8	6.0
Pd_{Escat}	5.00	2.8 ± 0.8	6	1	41	58	41	n.d.	n.d.	-

[a)] from TEM, at least 300 particles; [b)] number ratio; [c)] from TEM, at least 500 elements; [d)] calculated, see experimental details; [e)] from XPS measurements; [f)] Calculations based on the small mean particle size give a value of 100% for dispersion. Because larger particles are effectively present, we choose to be conservative by indicating >95% when discussing these highly dispersed catalysts.

The aberration-corrected HAADF-STEM images (Fig. 2) show Pd SA and NP co-existence, even on the reference Pd_{Escat} and Pd_2 catalysts. The uncontrolled presence of Pd SA with Pd NP on conventional or commercial Pd/C catalysts may be common for a long time, but their detection and the idea that they may play a role in catalysis is recent [40]. Fig. 3 presents particle size distributions obtained for the different catalysts. The two reference catalysts, Pd_2 and Pd_{Escat}, show larger mean particle sizes (2.2 and 2.8 nm, respectively) and lower SA/NP ratio (2.0 and 6.0) because of their higher Pd loading but also their conventional "uncontrolled" preparation. The four other catalysts present smaller mean particle sizes in the 0.5 – 1.1 nm range, depending on the SA/NP ratio and very high Pd dispersion. Increasing the number of Pd deposition cycles (see experimental section) induces an increase in the mean Pd NP size and a decrease in the SA/NP ratio. STEM-HAADF provides only a very local analysis of the samples (poor statistic value), so the catalyst series was also characterized by XPS. XPS can distinguish Pd NP and Pd SA due to differences in their oxidation states explained by the charge transfer between the carbon support and the metallic atoms anchored on it (Fig. S1) [36]. A reasonable correlation between the fraction of SA determined from TEM and the $Pd^{\delta+}$ fraction determined by XPS was obtained (Table 1 and Fig. S2).

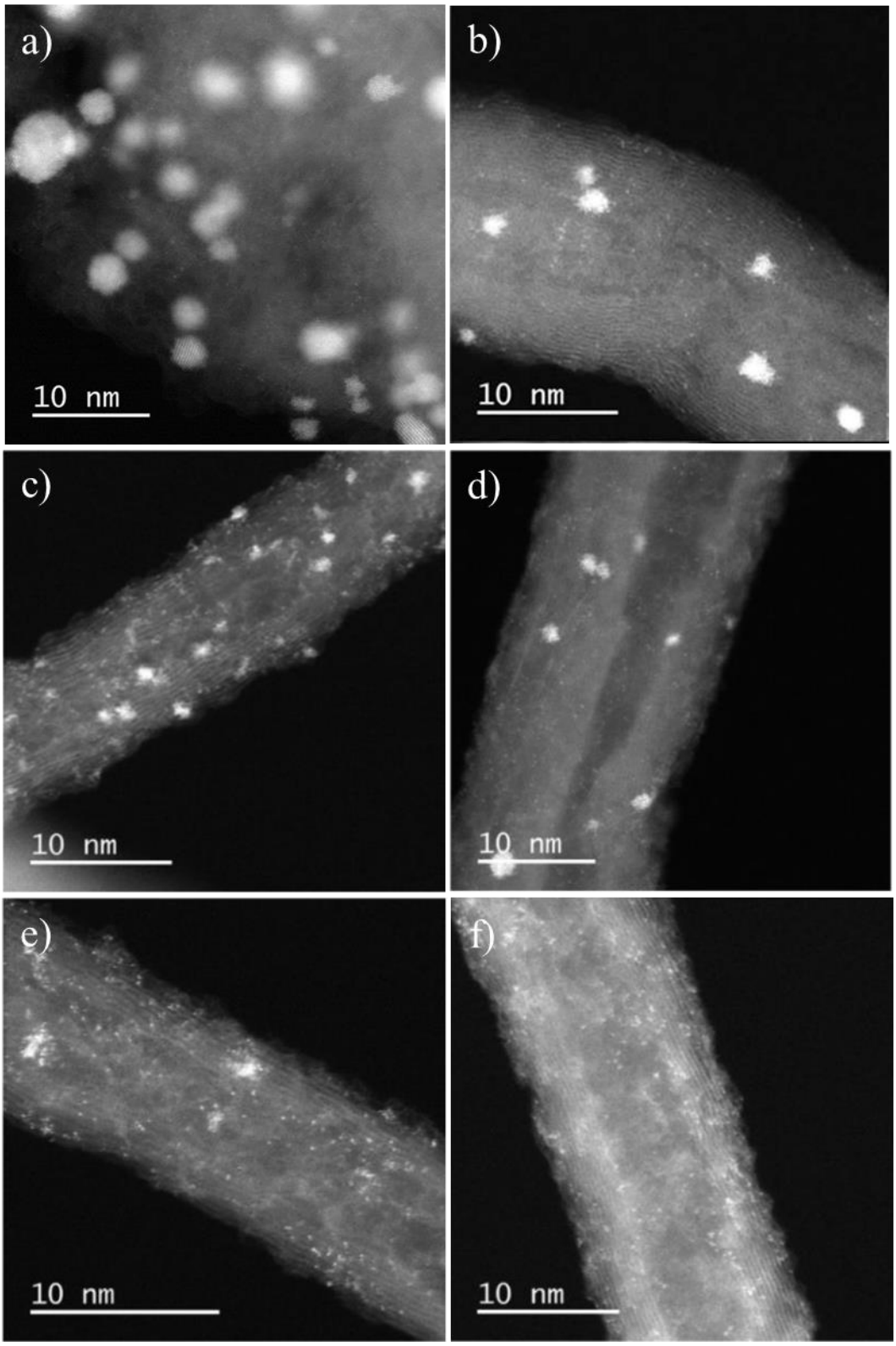

Fig. 2. STEM-HAADF analysis of palladium catalysts: a) Pd_{Escat}; b) Pd_2; c) Pd_{10}; d) Pd_{40}; e) Pd_{60}; and f) Pd_{200}

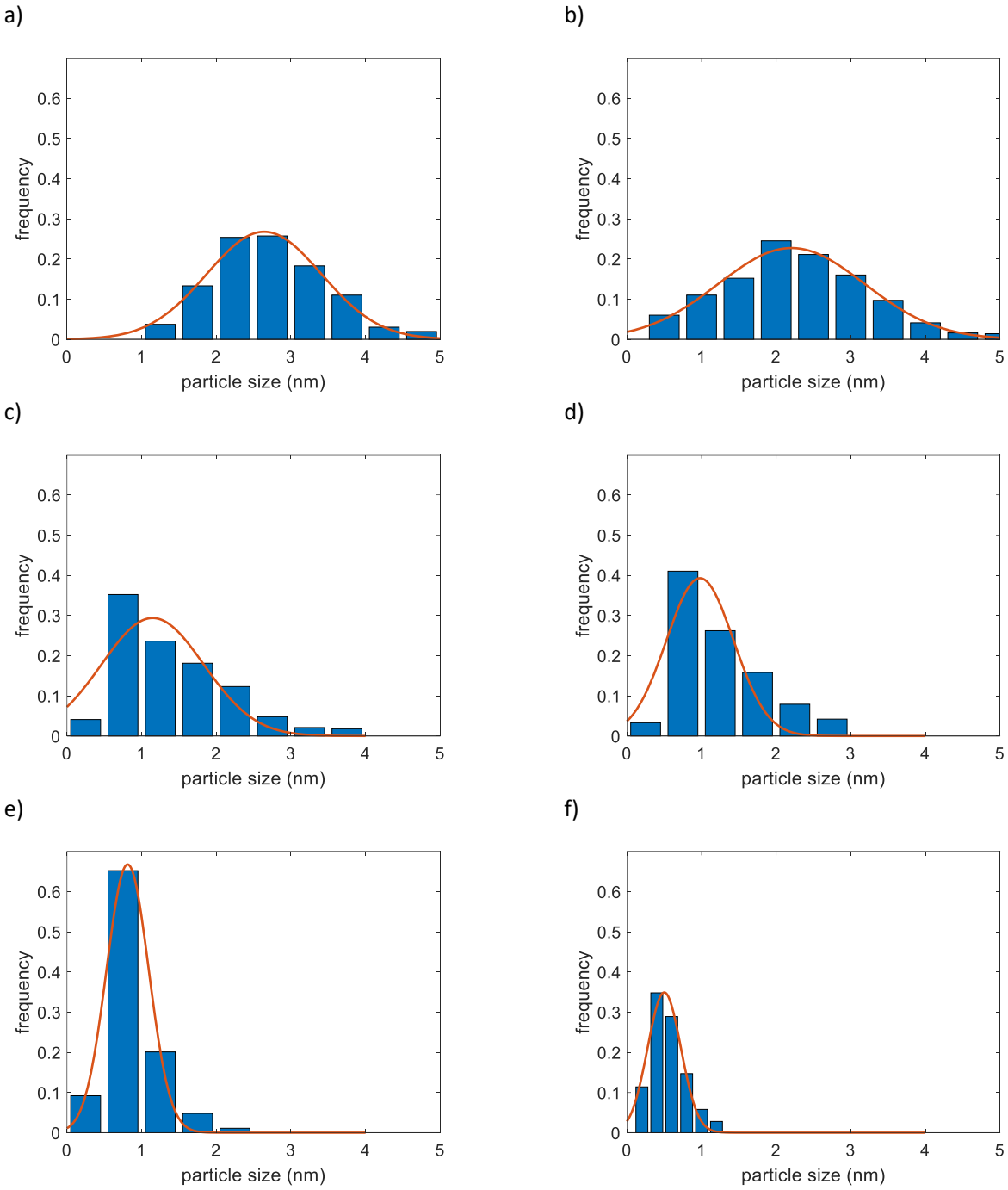

Fig. 3. Particle size distribution for the catalyst: a) Pd_{Escat}; b) Pd_2; c) Pd_{10}; d) Pd_{40}; e) Pd_{60}; and f) Pd_{200}. The orange lines are the Gaussian fits of the obtained distributions.

3.2. Catalytic studies

The catalytic performance of the reference PdEscat catalyst was evaluated in the reduction of AP in a stirred tank reactor. The absence of noticeable internal or external (Gas-Liquid or Liquid-Solid) mass transfer resistances has been checked (See supporting information S2), and the recovered data are consistent with intrinsic kinetics in chemical regime. In order to precisely study the behavior of the catalyst, the composition of the reaction as the function of time needs to be precisely determined. This could be done by ex-situ analysis by periodical liquid sampling for subsequent GC-FID analysis. Fig. 4a depicts a typical profile obtained according to this classical reaction progress monitoring. However, even if this procedure gives valuable results, the sampling frequency must be adapted to the activity of the studied catalyst. The hydrogen consumption evolution is another complementary data that can help study the catalyst's activity. This data is obtained indirectly by monitoring the H_2 pressure ($P_{H_2}^{res}$) and temperature (Tres) in the reservoir at a 1 Hz frequency. This monitoring was used to determine the corresponding H_2 uptake evolution by the reactive media (Fig. 4b). The hydrogen consumption was systematically checked to be in good agreement with the mass balance determined using GC/FID analysis of the reaction mixture.

Fig. 4a and 4b show that AP reacts through two successive reactions: hydrogenation of AP to the corresponding PE followed by hydrogenolytic rupture of the C–O bond, yielding EB (Fig. 1). Unlike experiments with Pd supported on various supports, no styrene was identified as intermediate under our conditions. This could be explained by the lower reaction temperature, 60°C vs. 130°C [20]. No hydrogenolysis reaction could be observed until an AP conversion higher than 80%. This could be explained by the stronger adsorption of AP on the active phase compared to PE. An apparent partial order in AP of zero for conversion up to 80% was observed (Fig. 4a). Then, the hydrogenolysis reaction started (Fig. 1), showing an apparent partial order in PE close to 1.

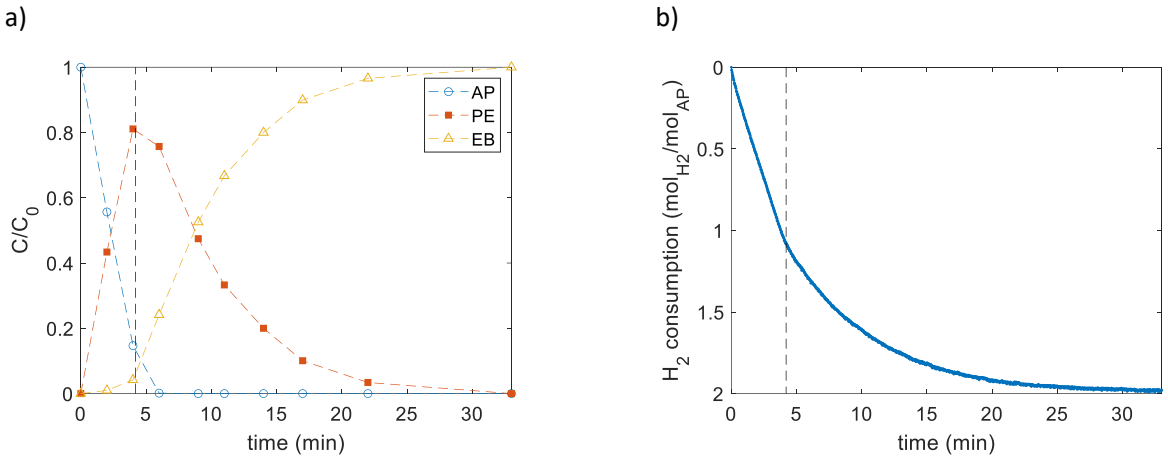

Fig. 4. a) Composition profile of the liquid phase; and b) corresponding H_2 reserve pressure consumption profile as the function of time during the hydrogenation of AP. Experimental conditions: 0.2 M AP in EtOH, 5 bar H_2, 60 °C, Pd_{Escat}, 0.2 mol% Pd.

3.3. Kinetic modeling

In the following, hydrogen uptake and liquid composition profiles will be used to precisely fit the kinetic constants of an appropriate model for these two reactions. This method appears interesting because a practical and quantitative catalyst activity comparison can be provided based on a limited set of kinetic parameters. Moreover, the modeling approach helps correctly handle catalyst activity when both reactions occur simultaneously, near the optimum.

Although most of the publications on AP reduction have focused on screening new catalysts and improving catalytic properties, only a few studies have addressed the development of kinetic models for this reaction [3,5,6,9,20]. Unfortunately, the experimental conditions used in these works (solvent, temperature, pressure) and the active metal used are different. Therefore, starting from these published data, a detailed set of experiments has been conducted on the Pd_{Escat} reference catalyst to select the most appropriate global kinetic description using the Langmuir-Hinshelwood-Hougen-Watson (LHHW) formalism. A wide experimental domain has been explored, including variations in the concentration (0.2 to 0.8 M) of starting reactant (AP), intermediate (PE), and final products (EB and water). The influence of H_2 pressure (2 to 15 bar) has also been experienced (see supporting information S3, Table S5). The best fit was obtained when considering the competitive adsorption of AP and PE associated with a non-competitive and dissociative adsorption for H_2 in the hydrogenation step. For the hydrogenolysis step, a non-dissociative H_2 activation and competitive adsorption between AP, PE, EB, and H_2 are required to represent the data well. This kinetic model is similar to the one derived in the work of Bergault *et al* [6] for a Rh/C catalyst. The corresponding kinetic rate expressions are given in equations (2) and (3), making use of 6 kinetic parameters (K_{AC}, K_{PE}, K_{EB}+K_{H_2O}, K_{H_2}, $k_{hydrogenation}$, and $k_{hydrogenolysis}$). Table 2 presents the values of the 6 regressed kinetic parameters in the case of this reference Pd_{Escat} catalyst, and Fig. S5 depicts the parity plots for liquid phase composition and H_2 uptake, demonstrating the excellent ability of the model to represent experimental data. Table S6 shows that the regressed parameters are not significantly correlated.

$$r_{hydrogenation}(t) = k_{hydrogenation} \cdot \frac{K_{AC}.C_{AC}(t)}{1+K_{AC}.C_{AC}(t)+K_{PE}.C_{PE}(t)} \cdot \frac{(K_{H2}.P_{H2}(t))^{0.5}}{1+(K_{H2}.P_{H2}(t))^{0.5}} \quad (2)$$

$$r_{hydrogenolysis}(t) = k_{hydrogenolyse} \cdot \frac{K_{PE}.C_{PE}(t).K_{H2}.P_{H2}(t)}{(1+K_{AC}.C_{AC}(t)+K_{PE}.C_{PE}(t)+(K_{EB}+K_{H2O}).C_{EB}(t)+K_{H2}.P_{H2}(t))^2} \quad (3)$$

Table 2.

Optimized parameters of the LHHW kinetic model applied to the Pd_{Escat} reference catalyst with 95% confidence intervals.

K_{AC}	K_{PE}	K_{EB}+K_{H_2O}	K_{H_2}	$k_{hydrogenation}$	$k_{hydrogenolysis}$
$L \cdot mol^{-1}$	$L.mol^{-1}$	$L.mol^{-1}$	bar^{-1}	$mol.h^{-1}.mol_{surface\ Pd}^{-1}$	$mol.h^{-1}.mol_{surface\ Pd}^{-1}$
139 ± 9	9.0 ± 0.5	9.6 ± 0.6	0.54 ± 0.02	31600 ± 400	$82000 \cdot \pm 2000$

A similar experiment has been repeated for the different catalysts of this study with the following conditions: 0.2M AP in ethanol; 60 °C; 5 bar; Pd 0.03 mol%. The evolution of the liquid phase composition is presented in Fig. 5 a-e. Similar behaviors to the Pd_{Escat} catalyst are observed, with pseudo-zeroth order for the hydrogenation step and pseudo-first order for the hydrogenolysis one. Furthermore, noticeable differences in activity and selectivity near the optima in PE are present when the SA/NP ratio is changed.

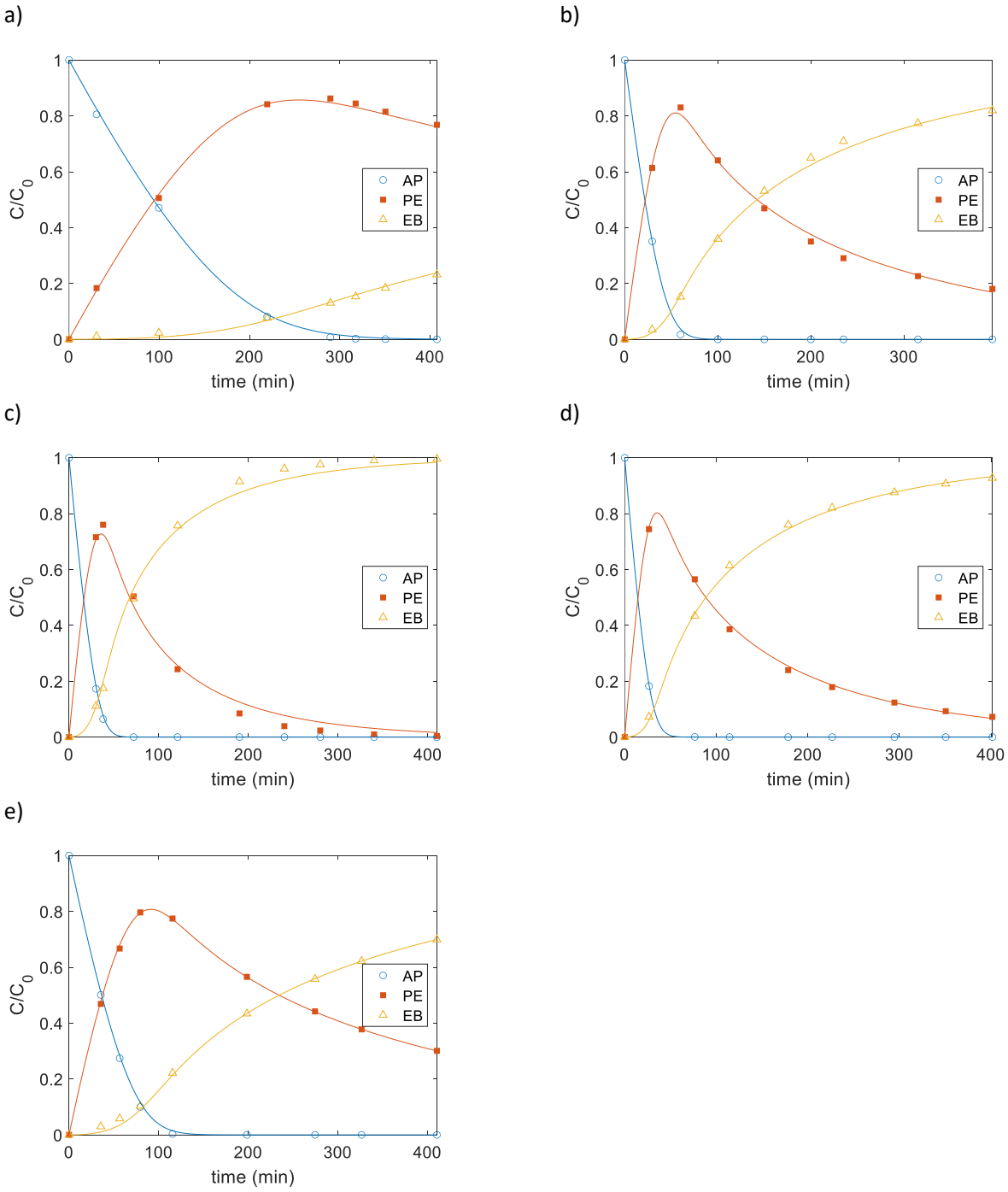

Fig. 5. Liquid phase composition evolution with time for the different catalysts of this study: a) Pd_{200}; b) Pd_{60}; c) Pd_{40}; d) Pd_{10}, and e) Pd_2. Characteristics of the Pd catalysts are listed in table 1. The lines are the results of the model fittings. Experimental conditions: 0.2M AP in EtOH, 60°C, 5 bars H_2, Pd 0.03 mol%.

3.4. Impact of the SA/NP ratio on the kinetics

To practically and quantitatively determine the impact of the SA/NP ratio and, thus the impact of the surface Pd distribution between SA and NP on the observed kinetics, the previous model developed for the Pd_{Escat} catalyst has been adjusted for each catalyst of this series. Because of a limited set of experimental data, the regression was reasonably limited to 4 parameters: $k_{hydrogenation}$, $k_{hydrogenolysis}$, and product adsorption parameters (K_{PE} and K_{EB}+K_{H2O}), while reactant adsorption parameters (K_{AP} and K_{H2} determined previously for the Pd_{Escat} catalyst) have been assumed constant. This limited fitting allows a low correlation between the regressed parameters (Table S7) and a good fit of a limited data set. The continuous lines in Fig. 5a-e are the results of these fittings.

Fig. 6 presents the parity plot obtained for all the liquid composition profiles for all these catalysts. It confirms the excellent ability of this modeling approach to represent the experimental data. It is noteworthy that this is a first approach to quantify the impact of the SA/NP ratio on the kinetic of these reactions. A micro-kinetic approach considering the different types of sites, Pd SA and Pd NP, and the hydrogen spillover step would be of greater interest but cannot yet be implemented and would require very specific experiments that are not the object of this work.

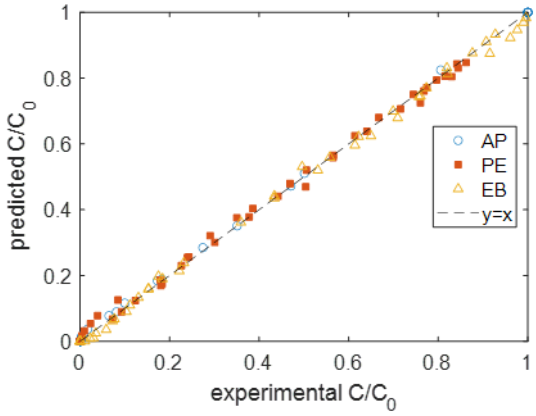

Fig. 6. Parity plot showing the experimental composition of the liquid phase vs. predicted concentration for the Pd/CNT series. Experimental conditions: 0.2M AP in EtOH, 60°C, 5 bars H_2, Pd 0.03 mol%.

Table 3 presents the results of the regressed parameters. They allow for quantitatively discussing the impact of the distribution of Pd between SA and NP on the observed catalyst activity and selectivity. Fig. 7 depicts these different kinetic constants graphically as the function of the atomic fraction of SA relative to the total surface atom of Pd.

Table 3.

Optimized parameters of the LHHW kinetic model applied to the different Pd/CNT catalysts with 95% confidence intervals.

Catalyst	K_{AC}	K_{PE}	$K_{EB}+K_{H2O}$	K_{H2}	$k_{hydrogenation}$	$k_{hydrogenolysis}$
	$L \cdot mol^{-1}$	$L.mol^{-1}$	$L.mol^{-1}$	bar^{-1}	$mol.h^{-1}.mol_{surface\ Pd}^{-1}$	$mol.h^{-1}.mol_{surface\ Pd}^{-1}$
Pd_2					6400 ± 200	9900 ± 400
Pd_{10}					14200 ± 900	23000 ± 2000
Pd_{40}	139 ± 9	33 ± 7	75 ± 9	0.54 ± 0.02	10500 ± 700	32000 ± 3000
Pd_{60}					8000 ± 500	12000 ± 1000
Pd_{200}					1900 ± 100	1700 ± 200

Significant variations of the activities of the catalysts are observed and quantified for the 2 considered reactions and these 5 different SA/NP ratios. The non-linear behavior observed when varying the distribution of Pd between SA and NP confirms the cooperative effects of SA and NP already stated (but not quantified) in the literature [41]. This effect is quantified here, and the concept is extended to the second consecutive reaction. Moreover, the present study clearly demonstrates that the presence of SA in the catalyst is insufficient to obtain higher catalytic performance, but it is crucial to control the ratio between SA and NP to obtain optimal catalytic activity. When considering the hydrogenation step, moving from a ratio of 2 (catalyst with a significant number of NP) to a ratio of 10 implies a twofold increase in the kinetic constant, confirming the critical role of this parameter in obtaining very cooperative active catalysts.

Interestingly, different optimal ratios are reached for the two consecutive reactions (Fig. 7). An optimal ratio of 10 (corresponding to an atomic fraction of Pd in the SA of 17%) is obtained for the hydrogenation of AP. An optimal ratio close to 40 (corresponding to an atomic fraction of Pd in the SA of 58%) for the hydrogenolysis of PE (Fig. 7). These values are probably correlated to the nature of the support and its ability to promote hydrogen spillover [37,44,45]. The justifications for the optimal value of this Pd SA/NP ratio are still unclear and will be further investigated in a separate work. Micro-kinetics data and mechanistic insights from DFT calculations should be necessary to understand the contribution of Pd SA and Pd NP, as well as the influence of the hydrogen spillover on the reduction of carbonyls. Finally, as expected, moving to very high values of atomic fraction of SA, the catalytic activities decrease for both reactions, confirming the tendencies observed in the literature for catalysts containing mainly single atoms [29,30,36].

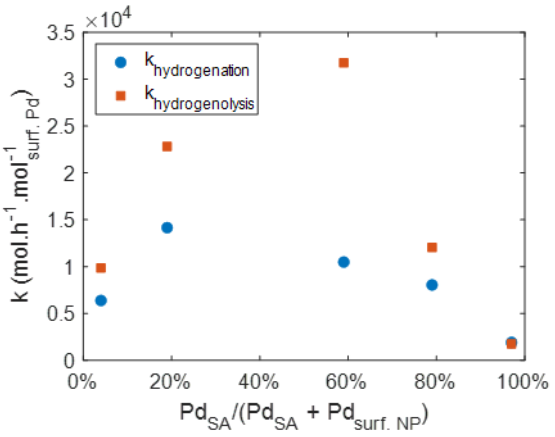

Fig. 7. Kinetic constants for the hydrogenation of AP to PE and for the hydrogenolysis of PE to EB as a function of the atomic fraction of SA for the Pd/CNT series. Experimental conditions: 0.2M AP in EtOH, 60°C, 5 bars H_2, Pd 0.03 mol%.

Fig. 8a shows the profiles of PE selectivity as the function of AP conversion. As expected, the selectivity toward PE remains the highest at high conversion for the catalyst Pd_{200}, having the highest fraction of Pd in the SA form (> 95%). The lowest selectivity-conversion profile is observed for the catalyst Pd_{40}. These results are in good agreement with Fig. 8b, which depicts the ratio between hydrogenation and hydrogenolysis kinetic parameters as a function of the atomic fraction of surface Pd in the form of SA for the different Pd/CNT catalysts. It indicates a good ability of the global modeling approach to handle and quantify the differences observed between catalysts near the optimum.

a)

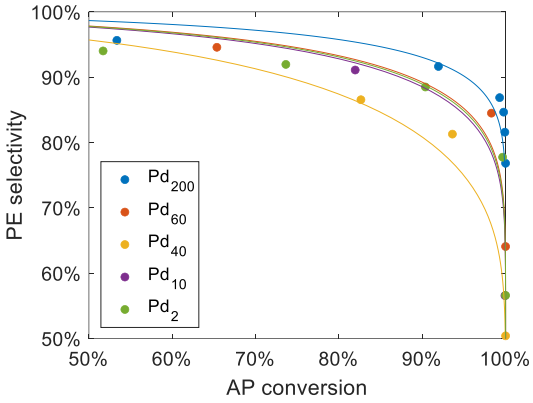

b)

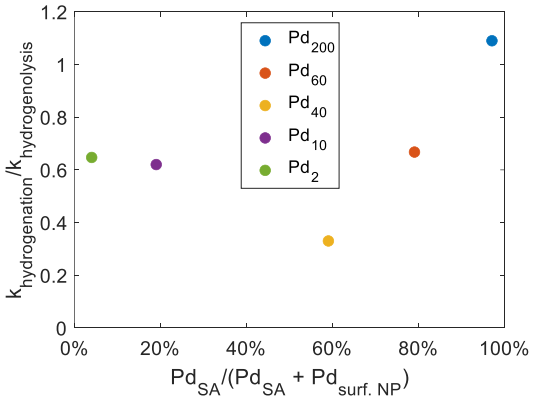

Fig. 8. a) Selectivity toward PE as the function of AP conversion for the Pd/CNT series. Characteristics of the Pd catalysts are listed in table 1. The lines are the results of the model fittings. b) Ratio between hydrogenation and hydrogenolysis fitted kinetic parameters as the function of the atomic fraction of Pd present in the SA. Experimental conditions: 0.2M AP in EtOH, 60 °C, 5 bars H_2, Pd 0.03 mol%.

4. Conclusion

Well-defined Pd catalysts supported on CNT with a controlled SA/NP ratio were evaluated for the reduction of acetophenone. This study demonstrates that the kinetic constants of the reduction to phenyl ethanol and further hydrogenolysis to ethyl benzene are largely impacted by the SA/NP ratio of the catalysts. This result could be linked to the cooperativity between the two kinds of active sites thanks to hydrogen spillover on the functionalized CNT support. Additionally, the optimum ratio changed for the two hydrogenation and hydrogenolysis steps. Such a controlled active phase tuning is expected to pave the way to very efficient catalysts involving supported metal single atoms. A thorough study of the theoretical mechanism of acetophenone hydrogenation is in progress to discuss further the possible micro-mechanism involved. In addition, the presence of clusters and cluster size impact on the catalytic performance should be further studied.

CRediT authorship contribution statement

Vincent Bernardin: Investigation, Methodology, Data curation, Visualization. Laurent Vanoye: Methodology, Data curation, Visualization. Camila Rivera-Cárcamo: Investigation, Catalysts synthesis and characterization. Philippe Serp: Resources, Project administration, Methodology, Writing – review & editing. Alain Favre-Réguillon: Methodology, Supervision, Writing – review & editing. Régis Philippe: Resources, Project administration, Methodology, Supervision, Visualization, Writing - Review & Editing.

Declaration of Competing Interest

The authors declare that they have no known competing financial interests or personal relationships that could have appeared to influence the work reported in this paper.

Data Availability

Data will be made available on request.

Acknowledgments

This work was supported by the French "Agence Nationale de la Recherche" (project ANR-19-CE07-0030, COMET), which is gratefully acknowledged. Frédéric Bornette is acknowledged for contributing to the experimental setup and the development of the acquisition tools.

References

[1] D.C. Costa, J.F. Bengoa, S.G. Marchetti, V. Vetere, Impact of the surface hydrophobicity/hydrophilicity ratio on the catalytic properties of Ni nanoparticles/MCM-41 system used in the hydrogenation of acetophenone, Catal. Today, 372 (2021) 20-26.

[2] Y. Gou, X. Liang, B. Chen, Catalytic hydrogenation of acetophenone over shape controlled Pd catalysts supported on sheet-like NiO, Catal. Today, 216 (2013) 200-204.

[3] M.V. Rajashekharam, I. Bergault, P. Fouilloux, D. Schweich, H. Delmas, R.V. Chaudhari, Hydrogenation of acetophenone using a 10% Ni supported on zeolite Y catalyst: kinetics and reaction mechanism, Catal. Today, 48 (1999) 83-92.

[4] B. Wang, M. Jin, H. An, Z. Guo, Z. Lv, Hydrogenation Performance of Acetophenone to 1-Phenylethanol on Highly Active Nano Cu/SiO_2 Catalyst, Catal. Lett., 150 (2019) 56-64.

[5] S. Lee, Z. Yu, N. Zaborenko, A. Varma, Acetophenone hydrogenation on Rh/Al_2O_3 catalyst: Intrinsic reaction kinetics and effects of internal diffusion, Chem. Eng. J., 288 (2016) 711-723.

[6] I. Bergault, P. Fouilloux, C. Joly-Vuillemin, H. Delmas, Kinetics and intraparticle diffusion modelling of a complex multistep reaction: Hydrogenation of acetophenone over a rhodium catalyst, J. Catal., 175 (1998) 328-337.

[7] M. Chen, N. Maeda, A. Baiker, J. Huang, Molecular Insight into Pt-Catalyzed Chemoselective Hydrogenation of an Aromatic Ketone by In Situ Modulation–Excitation IR Spectroscopy, ACS Catal., 2 (2012) 2007-2013.

[8] C.-S. Chen, H.-W. Chen, W.-H. Cheng, Study of selective hydrogenation of acetophenone on Pt/SiO_2, Appl. Catal., A, 248 (2003) 117-128.

[9] F. Gao, A.D. Allian, H. Zhang, S. Cheng, M. Garland, Chemical and kinetic study of acetophenone hydrogenation over Pt/Al_2O_3: Application of BTEM and other multivariate techniques to quantitative on-line FTIR measurements, J. Catal., 241 (2006) 189-199.

[10] R. Paul, S.C. Shit, T. Fovanna, D. Ferri, B. Srinivasa Rao, G. Gunasooriya, D.Q. Dao, Q.V. Le, I. Shown, M.P. Sherburne, Q.T. Trinh, J. Mondal, Realizing Catalytic Acetophenone Hydrodeoxygenation with Palladium-Equipped Porous Organic Polymers, ACS Appl. Mater. Interfaces, 12 (2020) 50550-50565.

[11] C. Sumner, W. Burchett, Developments in the Pd Catalyzed Hydrogenation of Oxygenated Organic Compounds, Top. Catal., 55 (2012) 480-485.

[12] Y.-Z. Xiang, Y.-A. Lv, T.-Y. Xu, X.-N. Li, J.-G. Wang, Selectivity difference between hydrogenation of acetophenone over CNTs and ACs supported Pd catalysts, J. Mol. Catal. A: Chem., 351 (2011) 70-75.

[13] M. Chen, N. Maeda, A. Baiker, J. Huang, Hydrogenation of Acetophenone on Pd/Silica–Alumina Catalysts with Tunable Acidity: Mechanistic Insight by In Situ ATR-IR Spectroscopy, ACS Catal., 8 (2018) 6594-6600.

[14] K.D. Kim, Z. Wang, Y. Tao, H. Ling, Y. Yuan, C. Zhou, Z. Liu, M. Gaborieau, J. Huang, A. Yu, The Comparative Effect of Particle Size and Support Acidity on Hydrogenation of Aromatic Ketones, ChemCatChem, 11 (2019) 4810-4817.

[15] W. Alsalahi, W. Tylus, A.M. Trzeciak, Highly selective hydrogenation of aromatic ketones to alcohols in water: effect of PdO and ZrO_2, Dalton Trans, 50 (2021) 10386-10393.

[16] Z. Wang, S. Pokhrel, M. Chen, M. Hunger, L. Mädler, J. Huang, Palladium-doped silica–alumina catalysts obtained from double-flame FSP for chemoselective hydrogenation of the model aromatic ketone acetophenone, J. Catal., 302 (2013) 10-19.

[17] Y. Zhang, S. Zhan, K. Liu, M. Qiao, N. Liu, R. Qin, L. Xiao, P. You, W. Jing, N. Zheng, Heterogeneous Hydrogenation with Hydrogen Spillover Enabled by Nitrogen Vacancies on Boron Nitride-Supported Pd Nanoparticles, Angew. Chem. Int. Ed., (2023) e202217191.

[18] S.R. More, G.D. Yadav, Effect of Supercritical CO2 as Reaction Medium for Selective Hydrogenation of Acetophenone to 1-Phenylethanol, ACS Omega, 3 (2018) 7124-7132.

[19] C.-S. Chen, H.-W. Chen, Enhanced selectivity and formation of ethylbenzene for acetophenone hydrogenation by adsorbed oxygen on Pd/SiO_2, Appl. Catal., A, 260 (2004) 207-213.

[20] M. Bejblová, P. Zámostný, L. Červený, J. Čejka, Hydrogenation and hydrogenolysis of acetophenone, Collect. Czech. Chem. Commun., 68 (2003) 1969-1984.

[21] R. Paul, S.C. Shit, T. Fovanna, D. Ferri, B. Srinivasa Rao, G.T.K.K. Gunasooriya, D.Q. Dao, Q.V. Le, I. Shown, M.P. Sherburne, Q.T. Trinh, J. Mondal, Realizing Catalytic Acetophenone Hydrodeoxygenation with Palladium-Equipped Porous Organic Polymers, ACS Appl. Mater. Interfaces, 12 (2020) 50550-50565.

[22] A. Wang, J. Li, T. Zhang, Heterogeneous single-atom catalysis, Nat. Rev. Chem., 2 (2018) 65-81.

[23] S. Liang, C. Hao, Y. Shi, The Power of Single-Atom Catalysis, ChemCatChem, 7 (2015) 2559-2567.

[24] Z.-Y. Li, Z. Yuan, X.-N. Li, Y.-X. Zhao, S.-G. He, CO Oxidation Catalyzed by Single Gold Atoms Supported on Aluminum Oxide Clusters, J. Am. Chem. Soc., 136 (2014) 14307-14313.

[25] L. Sun, J. Xu, X. Liu, B. Qiao, L. Li, Y. Ren, Q. Wan, J. Lin, S. Lin, X. Wang, H. Guo, T. Zhang, High-Efficiency Water Gas Shift Reaction Catalysis on α-MoC Promoted by Single-Atom Ir Species, ACS Catal., 11 (2021) 5942-5950.

[26] S. Tao, D. Yang, M. Wang, G. Sun, G. Xiong, W. Gao, Y. Zhang, Y. Pan, Single-atom catalysts for hydroformylation of olefins, iScience, 26 (2023) 106183.

[27] Q. Zhang, J. Guan, Single-Atom Catalysts for Electrocatalytic Applications, Adv. Funct. Mater., 30 (2020) 2000768.

[28] L. Zhang, M. Zhou, A. Wang, T. Zhang, Selective Hydrogenation over Supported Metal Catalysts: From Nanoparticles to Single Atoms, Chem. Rev., 120 (2020) 683-733.

[29] M.D. Rossell, F.J. Caparrós, I. Angurell, G. Muller, J. Llorca, M. Seco, O. Rossell, Magnetite-supported palladium single-atoms do not catalyse the hydrogenation of alkenes but small clusters do, Catal. Sci. Technol., 6 (2016) 4081-4085.

[30] J. Yang, X. Du, B. Qiao, Comprehensive activity evaluation of single-atom catalysts, Chem Catalysis, 3 (2023) 100424.

[31] S. Büchele, Z. Chen, S. Mitchell, R. Hauert, F. Krumeich, J. Pérez-Ramírez, Tailoring Nitrogen-Doped Carbons as Hosts for Single-Atom Catalysts, ChemCatChem, 11 (2019) 2812-2820.

[32] Y. Liu, B. Wang, Q. Fu, W. Liu, Y. Wang, L. Gu, D. Wang, Y. Li, Polyoxometalate-Based Metal–Organic Framework as Molecular Sieve for Highly Selective Semi-Hydrogenation of Acetylene on Isolated Single Pd Atom Sites, Angew. Chem. Int. Ed., 60 (2021) 22522-22528.

[33] X. Tao, B. Nan, Y. Li, M. Du, L.-l. Guo, C. Tian, L. Jiang, L. Shen, N. Sun, L.-N. Li, Highly Active Isolated Single-Atom Pd Catalyst Supported on Layered MgO for Semihydrogenation of Acetylene, ACS Appl. Energy Mater., 5 (2022) 10385-10390.

[34] X. Huang, H. Yan, L. Huang, X. Zhang, Y. Lin, J. Li, Y. Xia, Y. Ma, Z. Sun, S. Wei, J. Lu, Toward Understanding of the Support Effect on Pd_1 Single-Atom-Catalyzed Hydrogenation Reactions, J. Phys. Chem. C, 123 (2019) 7922-7930.

[35] H. Yan, H. Cheng, H. Yi, Y. Lin, T. Yao, C. Wang, J. Li, S. Wei, J. Lu, Single-Atom Pd_1/Graphene Catalyst Achieved by Atomic Layer Deposition: Remarkable Performance in Selective Hydrogenation of 1,3-Butadiene, J. Am. Chem. Soc., 137 (2015) 10484-10487.

[36] C. Rivera-Cárcamo, I.C. Gerber, I. del Rosal, B. Guicheret, R. Castro Contreras, L. Vanoye, A. Favre-Réguillon, B.F. Machado, J. Audevard, C. de Bellefon, R. Philippe, P. Serp, Control of the single atom/nanoparticle ratio in Pd/C catalysts to optimize the cooperative hydrogenation of alkenes, Catal. Sci. Technol., 11 (2021) 984-999.

[37] P. Serp, Cooperativity in supported metal single atom catalysis, Nanoscale, 13 (2021) 5985-6004.

[38] W. Gao, S. Liu, G., Sun, C. Zhang, Y. Pan, Single-Atom Catalysts for Hydrogen Activation. Small 2023, 2300956.

[39] C. Chu, D. Huang, S. Gupta, S. Weon, J. Niu, E. Stavitski, C. Muhich, J.-H. Kim, Neighboring Pd single atoms surpass isolated single atoms for selective hydrodehalogenation catalysis, Nat. Commun., 12 (2021) 5179.

[40] U. Petek, F. Ruiz-Zepeda, M. Bele, M. Gaberšček, Nanoparticles and Single Atoms in Commercial Carbon-Supported Platinum-Group Metal Catalysts, Catalysts, 9 (2019) 134.

[41] L. Kuai, Z. Chen, S. Liu, E. Kan, N. Yu, Y. Ren, C. Fang, X. Li, Y. Li, B. Geng, Titania supported synergistic palladium single atoms and nanoparticles for room temperature ketone and aldehydes hydrogenation, Nat. Commun., 11 (2020) 48.

[42] J. Yang, L. Yang, L. Zhang, T. Yu, D. Zhai, H. Wang, W. Zhou, Y. Li, G. Ren, L. Sun, W. Deng, Hydrogenation Reactions with Synergistic Catalysis of Pd single atoms and nanoparticles under Near-Ambient Conditions, Chem. Eur. J., (2022) e202203108.

[43] R. Prins, Hydrogen Spillover. Facts and Fiction, Chem. Rev., 112 (2012) 2714-2738.

[44] L. Warczinski, C. Hättig, How Nitrogen Doping Affects Hydrogen Spillover on Carbon-Supported Pd Nanoparticles: New Insights from DFT, J. Phys. Chem. C, 125 (2021) 9020-9031.

[45] I.C. Gerber, P. Serp, A Theory/Experience Description of Support Effects in Carbon-Supported Catalysts, Chem. Rev., 120 (2020) 1250-1349.

[46] R.C. Contreras, B. Guicheret, B.F. Machado, C. Rivera-Cárcamo, M.A. Curiel Alvarez, B. Valdez Salas, M. Ruttert, T. Placke, A. Favre-Réguillon, L. Vanoye, C. de Bellefon, R. Philippe, P. Serp, Effect of mesoporous carbon support nature and pretreatments on palladium loading, dispersion and apparent catalytic activity in hydrogenation of myrcene, J. Catal., 372 (2019) 226-244.

[47] L. Vanoye, B. Guicheret, C. Rivera-Carcamo, R.C. Contreras, C. de Bellefon, V. Meille, P. Serp, R. Philippe, A. Favre-Reguillon, Process intensification of the catalytic hydrogenation of squalene using a Pd/CNT catalyst combining nanoparticles and single atoms in a continuous flow reactor, Chem. Eng. J., 441 (2022) 135951.

[48] B. Guicheret, L. Vanoye, C. Rivera-Carcamo, C. de Bellefon, P. Serp, R. Philippe, A. Favre-Reguillon, Solvent-Free Hydrogenation of Squalene Using Parts per Million Levels of Palladium Supported on Carbon Nanotubes: Shift from Batch Reactor to Continuous-Flow System, ChemSusChem, 15 (2022) e202200916.

[49] C.-T. Kuo, Y. Lu, L. Kovarik, M. Engelhard, A.M. Karim, Structure Sensitivity of Acetylene Semi-Hydrogenation on Pt Single Atoms and Subnanometer Clusters, ACS Catal., 9 (2019) 11030-11041.

[50] A. Borodziński, M. Bonarowska, Relation between Crystallite Size and Dispersion on Supported Metal Catalysts, Langmuir, 13 (1997) 5613-5620.

Acetophenone hydrogenation and consecutive hydrogenolysis with Pd/CNT catalysts: highlighting the synergy between single atoms and nanoparticles by kinetic modeling

Vincent Bernardin,[1] Laurent Vanoye,[1] Camila Rivera-Cárcamo,[2] Philippe Serp,[2*] Alain Favre-Réguillon[1,3*], Régis Philippe[1*]

[1]Catalyse Polymérisation Procédés & Matériaux (CP2M), Université Lyon, UMR 5128 CNRS – CPE Lyon – UCBL, 43 boulevard du 11 novembre 1918, F-69100 Villeurbanne (France).

E-mail: regis.philippe@lgpc.cpe.fr

[2]ENSIACET, Université de Toulouse, LCC CNRS-UPR 8241, F-31030 Toulouse, (France).

E-mail : philippe.serp@ensiacet.fr

[3]Département Chimie-Vivant-Santé, Conservatoire National des Arts et Métiers, 292 rue Saint Martin, F-75003 Paris, (France).

E-mail: favrereg@cnam.fr

ABSTRACT

Understanding the cooperative action of palladium nanoparticles (NP) and palladium single atoms (SA) supported on carbon nanotubes (CNT) is essential for developing more efficient supported transition metal catalysts. In this work, the comparison of a series of Pd-catalysts on CNT having the same palladium loading (~1.4 wt%) but involving different and controlled SA/NP ratios (between 2 and 200) is described. The hydrogenation of acetophenone into 1-phenylethanol and its consecutive hydrogenolysis to ethylbenzene are the chosen test reactions. Appropriate kinetic modeling of these two consecutive reactions was performed and allowed a quantitative assessment of the activity differences between catalysts as well as the demonstration of a synergy between the two palladium species (SA and NP). The maximum activity was clearly dependent on the distribution of the surface palladium between SA and NP, and interestingly, different optima for the two reactions are evidenced. This work may offer a new perspective for the design and synthesis of supported transition metal catalysts with targeted catalytic performance.

Keywords: Palladium single atom catalyst; Palladium nanoparticles; Carbon nanotubes; Acetophenone; Kinetic modeling; Hydrogen

1. Introduction

The catalytic hydrogenation of organic compounds containing a carbonyl group is important in the synthesis of fine chemicals, pharmaceuticals, dyes, and agrochemicals. Acetophenone (AP) is a model molecule for evaluating and comparing supported catalysts for such a reaction. So far, catalytic systems such as Ni [1-3], Cu [4], Rh [5,6], and Pt [7-9] have been successfully used in the hydrogenation of acetophenone, but supported Pd catalysts are commonly used in the reduction of AP [2,10-19]. Pd promotes the formation of 1-phenylethanol (PE) and ethylbenzene (EB) in two consecutive reactions (Fig. 1) [13,20,21].

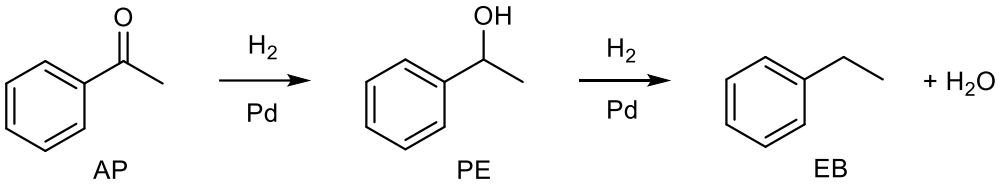

Fig. 1. Consecutive reactions steps involved in acetophenone hydrogenation and hydrogenolysis with Pd catalysts.

However, there are two problems related to the use of Pd. The first one is related to the lack of selectivity of the reaction, particularly related to the competition between the reduction and the hydrogenolysis steps. The second is related to the cost and the poor utilization of palladium in heterogeneous catalysts, which thus drives the search for alternatives. Recently, Pd single-atom (SA) catalysts have exhibited maximized atomic efficiency compared with conventional supported Pd nanoparticles (NP) catalysts due to 100 % metal dispersion and the presence of a single type of metal site [22]. SA catalysis demonstrated distinguishing performances [23], like CO oxidation [24], water gas shift reaction [25], hydroformylation [26], and electrocatalysis [27]. However, in the hydrogenation process [28], SA catalysts empower selectivity but at the expense of activity [29,30]. For instance, the specific properties of SA found valuable application in the selective hydrogenation of acetylene into ethylene [31-33] or 1,3-butadiene into butenes [34,35]. In contrast, the activities observed on double bonds, ketones, and even aldehydes are deceiving. This could be explained by the kinetically demanding dissociative pathway of H_2 on SA [36,37,38], especially if the substrate pre-coordinated SA sites [39].

Therefore, the improvement of the hydrogenation activity of Pd SA while maintaining its valuable properties has been addressed by different strategies. The first was to shorten the distance between SA so that two neighbouring SA provide adjacent active sites [39]. The properties of SA will be maintained while providing higher activity. The drawbacks of such a strategy are the large-scale preparation difficulties and the deactivation of atomically dispersed catalysts by sintering.

The second strategy was to use cooperativity between Pd SA and Pd NP [37,40-42]. H_2 dissociation is favoured on Pd NP compared to Pd SA, and hydrogen spillover on the support will enable the formation of the active H-Pd SA species [17,43-45]. We have reported a synthesis procedure of Pd catalysts supported on nano-structured carbon that allows controlling the SA/NP ratio [36,45]. These catalysts were demonstrated to be stable and highly active for alkenes hydrogenation [47,48].

The catalytic activities of these catalysts should depend on the combination of SA and NP [36], and the catalytic activities can be optimized by controlling such ratio. Herein, aiming to gain further insight into cooperativity between SA and NP, the performance of supported Pd on carbon nanotubes with different and controlled SA/NP ratio was studied for the hydrogenation/hydrogenolysis of acetophenone.

2. Experimental section

2.1. Catalysts and catalysts preparation

Pd_{Escat} (Strem chemicals, Product number Escat 1431) was used directly without further treatment. Pd_2 catalyst has been prepared using a classical wet impregnation method to obtain a high proportion of nanoparticles. The desired amount of palladium (II) nitrate dihydrate ($Pd(NO_3)_2.2H_2O$) (Sigma-Aldrich) was added to acetone (100 mL) containing 1 g of carbon nanomaterial to introduce 2 wt% of metal phase. The solution was sonicated at room temperature for 1 h and magnetically stirred overnight. The solution was then filtered and washed with acetone. The resulting solid was dried at 120 °C overnight. Finally, the Pd_2 catalyst was reduced in a horizontal furnace under a N_2/H_2 flow (20 vol% H_2) at 300 °C for 2 h (25°C to 300 °C at 10 °C/min).

Pd_{10}, Pd_{40}, Pd_{60}, and Pd_{200} catalysts have been prepared according to the procedure of P. Serp et al [36]. It consists of i) creating carboxylic groups on the support by nitric acid oxidation (step I), ii) decomposing these groups under an inert atmosphere to produce CO_2, some H_2 and carbon vacancies in the outer carbon nanotube layers (step II) and iii) depositing the metal on this defective and very reactive support (step III). For a given metal loading, if step III is performed once, mainly Pd SA are obtained; if it is performed several times (adjusting the amount of metal in each deposition), mixtures of SA and NP are obtained. The number of times that step III is performed for a given total metal loading modify the SA/NP ratio by increasing the relative number of NP. Bis (2-methylallyl)palladium precursor (Nanomeps) is used to perform these specific preparations. Its addition to the highly reactive activated CNT support containing the vacancies is done under an argon atmosphere and using an anhydrous pentane suspension of the support. At the end of each impregnation cycle, the precursor was decomposed under a N_2/H_2 flow (20 vol% H_2) at 80 °C for 1 h.

2.2. Catalysts characterization

The palladium content in the catalysts was determined by inductively coupled plasma optical emission spectroscopy (ICP-OES) performed at the LCC with a Thermo Scientific ICAP 6300 instrument. TEM and HR-TEM analyses were performed at the "Centre de microcaracterisation Raimond Castaing, UMS 3623, Toulouse" using a JEOL JEM 1011 CX-T electron microscope operating at 100 kV with a point resolution of 4.5 Å and a JEOL JEM 1400 electron microscope operating at 120 kV. The high-resolution analyses were conducted using a JEOL JEM 2100F equipped with a field emission gun (FEG) operating at 200 kV with a point resolution of 2.3 Å and a JEOL JEM-ARM200F Cold FEG operating at 200 kV with a point resolution of > 1.9 Å.

The particle size distribution was determined through several micrographs from different areas of the TEM grid (at least 300 particles). The size distributions reported as Pd atomic percentage (based on total atoms) in each size range were obtained by calculating the number of atoms (N) in each NP, assuming a spherical shape using an equation described in the literature [49]. The SA/NP ratio (a

number ratio) was measured from the STEM-HAADF analyses of at least 500 elements. Metal dispersion was evaluated from the fraction of SA and a universal mathematical relation between the mean relative size of metallic crystallites and their dispersion [50]. The samples were analysed by X-ray photoelectron spectroscopy (XPS) using a VG Escalab MKII spectrophotometer operating with a non-monochromatized Mg K source (1253.6 eV).

2.3. Reactivity measurements

Acetophenone catalytic hydrogenation was performed in a stirred tank reactor of 200 mL from Top Industrie. This reactor has 4 baffles and a gas-inducing Rushton turbine with 6 straight blades for efficient G-L-S contacting. Temperature control is provided by an electric shell (for heating) and a Ranque-Hilsch vortex device (for cooling). Typical catalytic tests were operated at 1200 rpm and 60 °C with 60 mg of Pd/CNT catalyst under an H_2 atmosphere at a constant pressure of 5 bar. The liquid phase consists of 120 mL of a 0.2 M acetophenone (Acros organics, 98%) solution in ethanol (VWR, absolute) previously purified by absorption on activated carbon. The reactor is thus operated in batch mode for the liquid and solid phases and in semi-batch mode for the gas because hydrogen was constantly fed via a pressure regulator and supplied by a calibrated and monitored reserve. Aliquots could be taken from the liquid phase and analyzed by GC-FID equipped with DB-1 and DB-WAX columns. The liquid phase temperature, the pressure inside the reactor, and the pressure and temperature of the reserve were acquired and recorded using Labview® at 1 Hz.

2.4. Kinetic and reactor modeling

Kinetic modeling studies were performed using Matlab® software (Matlab R2020b). A classical pseudo-homogeneous isothermal and isobaric stirred tank model has been used to simulate the liquid phase composition. The absence of physical limitations (G-L, L-S, and internal) has been verified thanks to classical chemical reaction engineering criteria and measurements (see supporting information). The Matlab routine is based on a Levenberg-Marquardt optimization algorithm and a Runge-Kutta solver. For the Pd_{Escat} catalyst, 6 kinetic parameters were adjusted and found significant and not correlated. For the comparison of the different catalysts, 4 kinetic constants were adjusted ($k_{hydrogenation}$, $k_{hydrogenolysis}$, K_{PE}, and K_{EB}+K_{H2O}), assuming the remaining adsorption parameters identical to the Pd_{Escat} reference catalyst. The objective function (OF) cleverly considers the complementary liquid composition and H_2 reserve consumption profiles with equal weight (see equation 1 below).

$$OF = \left\{ \sum_i \sum_j \sum_k \left(\frac{C_{i,j,k}^{L,theo} - C_{i,j,k}^{L,exp}}{C_{ref}} \right)^2 \right\} + \left\{ \sum_l \frac{\overline{N_L}}{N_{G,l}} \sum_m \left(\frac{n_{l,m}^{G,theo} - n_{l,m}^{G,exp}}{V_L \cdot C_{AP,l,0}^L} \right)^2 \right\} \quad (1)$$

In this equation, the first bracket refers to the liquid profiles involving "i" species in "j" experiments with "k" samplings. The second bracket corresponds to the H_2 consumption in "l" experiments with "m" data.

C_{ref} is a reference concentration of 0.2 mol/L; $\overline{N_L}$ is the average number of liquid sampling points for a single experiment; $N_{G,l}$ is the number of recorded pressure points in the experiment "l"; $C_{AP,l,0}^L$ is the initial AP concentration in the experiment "l". "L", "G", "theo", and "exp" superscripts refer to the liquid phase, the gas phase, theoretical and experimental values, respectively.

3. Results and Discussion

3.1. Synthesis and characterization

A series of Pd catalysts supported on carbon nanotubes were prepared by the method developed by P. Serp *et al* [36, 46]. The detailed characterization of the catalyst has been presented elsewhere [36], and Table 1**Erreur ! Source du renvoi introuvable.** summarizes the main characteristics of this series of catalysts conducted by STEM and XPS analyses. The Pd loading was set to ~1.4 wt% and the SA/NP ratio was varied from 10 to 200. This number ratio is recalled in the name of the catalyst. A commercial Pd/C catalyst (Pd_{Escat}) and a Pd/CNT catalyst containing mostly NP (Pd_2) have been taken as references for comparison.

Table 3.

Main characteristics of the investigated catalysts

Catalyst	Pd loading (wt%)	Average NP size[a)] (nm)	SA/NP ratio[b) c)] (-)	Pd in SA[c) d)] (atomic %)	Pd in NP surface[c) d)] (atomic %)	Pd in NP core[c) d)] (atomic %)	Dispersion[c) d)] (atomic %)	Pd^0 fraction[e)] (atomic %)	$Pd^{\delta+}$ fraction[e)] (atomic %)	$Pd^{\delta+}/Pd^0$ ratio[e)] (-)
Pd_2	2.04	2.2 ± 1.1	2	2	48	50	49	n.d.	n.d.	-
Pd_{10}	1.29	1.1 ± 0.6	10	17	74	9	89	41.8	58.2	1.4
Pd_{40}	1.43	0.9 ± 0.3	40	58	40[f)]	2[f)]	>95[f)]	22.0	78.0	3.5
Pd_{60}	1.37	0.8 ± 0.3	60	78	21[f)]	1[f)]	>95[f)]	15.2	84.7	5.5
Pd_{200}	1.33	0.5 ± 0.1	200	97	3[f)]	0[f)]	>95[f)]	14.2	85.8	6.0
Pd_{Escat}	5.00	2.8 ± 0.8	6	1	41	58	41	n.d.	n.d.	-

[a)] from TEM, at least 300 particles; [b)] number ratio; [c)] from TEM, at least 500 elements; [d)] calculated, see experimental details; [e)] from XPS measurements; [f)] Calculations based on the small mean particle size give a value of 100% for dispersion. Because larger particles are effectively present, we choose to be conservative by indicating >95% when discussing these highly dispersed catalysts.

The aberration-corrected HAADF-STEM images (Fig. 2) show Pd SA and NP co-existence, even on the reference Pd_{Escat} and Pd_2 catalysts. The uncontrolled presence of Pd SA with Pd NP on conventional or commercial Pd/C catalysts may be common for a long time, but their detection and the idea that they may play a role in catalysis is recent [40]. Fig. 3 presents particle size distributions obtained for the different catalysts. The two reference catalysts, Pd_2 and Pd_{Escat}, show larger mean particle sizes (2.2 and 2.8 nm, respectively) and lower SA/NP ratio (2.0 and 6.0) because of their higher Pd loading but also their conventional "uncontrolled" preparation. The four other catalysts present smaller mean particle sizes in the 0.5 – 1.1 nm range, depending on the SA/NP ratio and very high Pd dispersion. Increasing the number of Pd deposition cycles (see experimental section) induces an increase in the mean Pd NP size and a decrease in the SA/NP ratio. STEM-HAADF provides only a very local analysis of the samples (poor statistic value), so the catalyst series was also characterized by XPS. XPS can distinguish Pd NP and Pd SA due to differences in their oxidation states explained by the charge transfer between the carbon support and the metallic atoms anchored on it (Fig. S1) [36]. A reasonable correlation between the fraction of SA determined from TEM and the $Pd^{\delta+}$ fraction determined by XPS was obtained (Table 1 and Fig. S2).

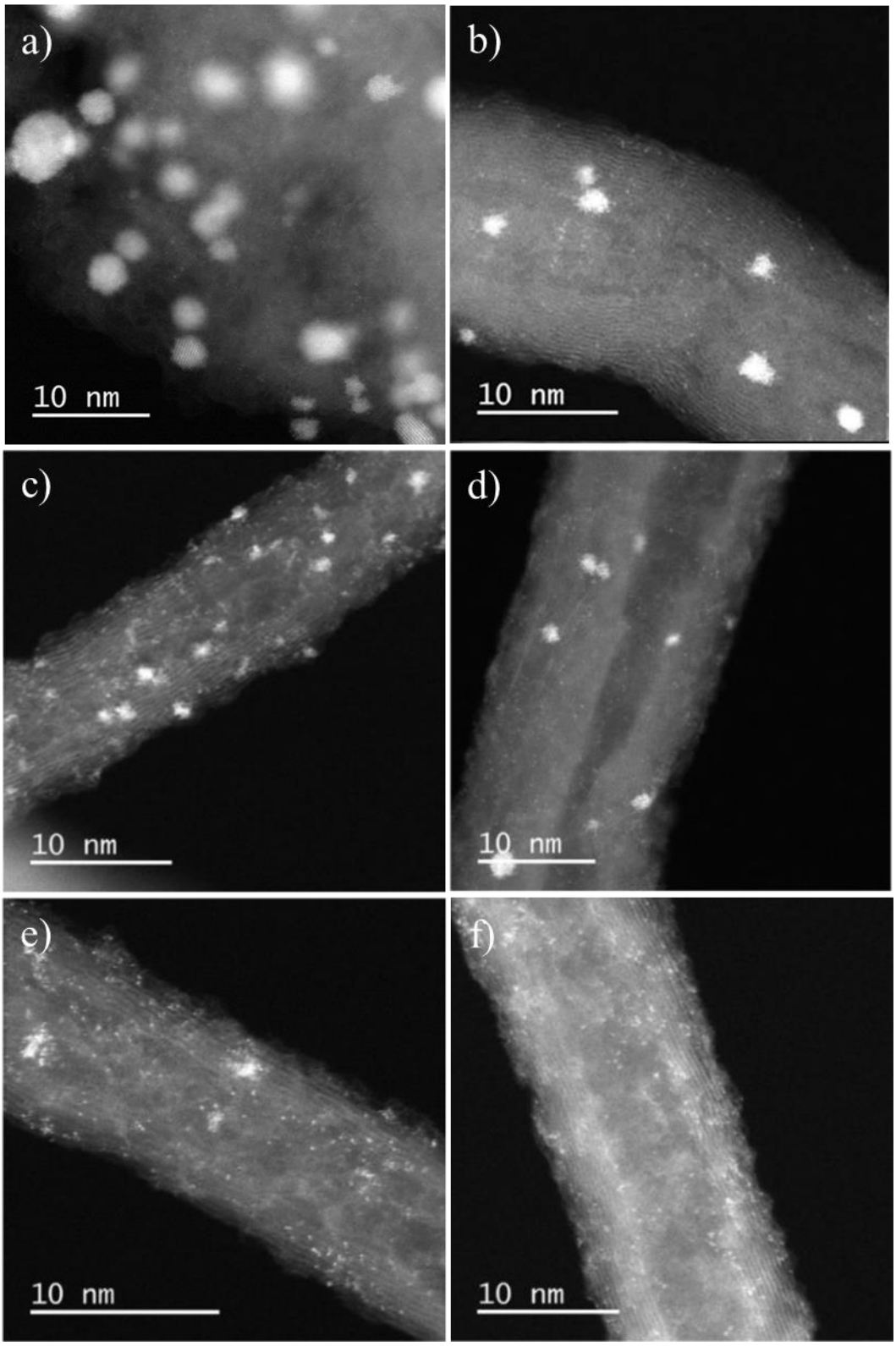

Fig. 2. STEM-HAADF analysis of palladium catalysts: a) Pd_{Escat}; b) Pd_2; c) Pd_{10}; d) Pd_{40}; e) Pd_{60}; and f) Pd_{200}

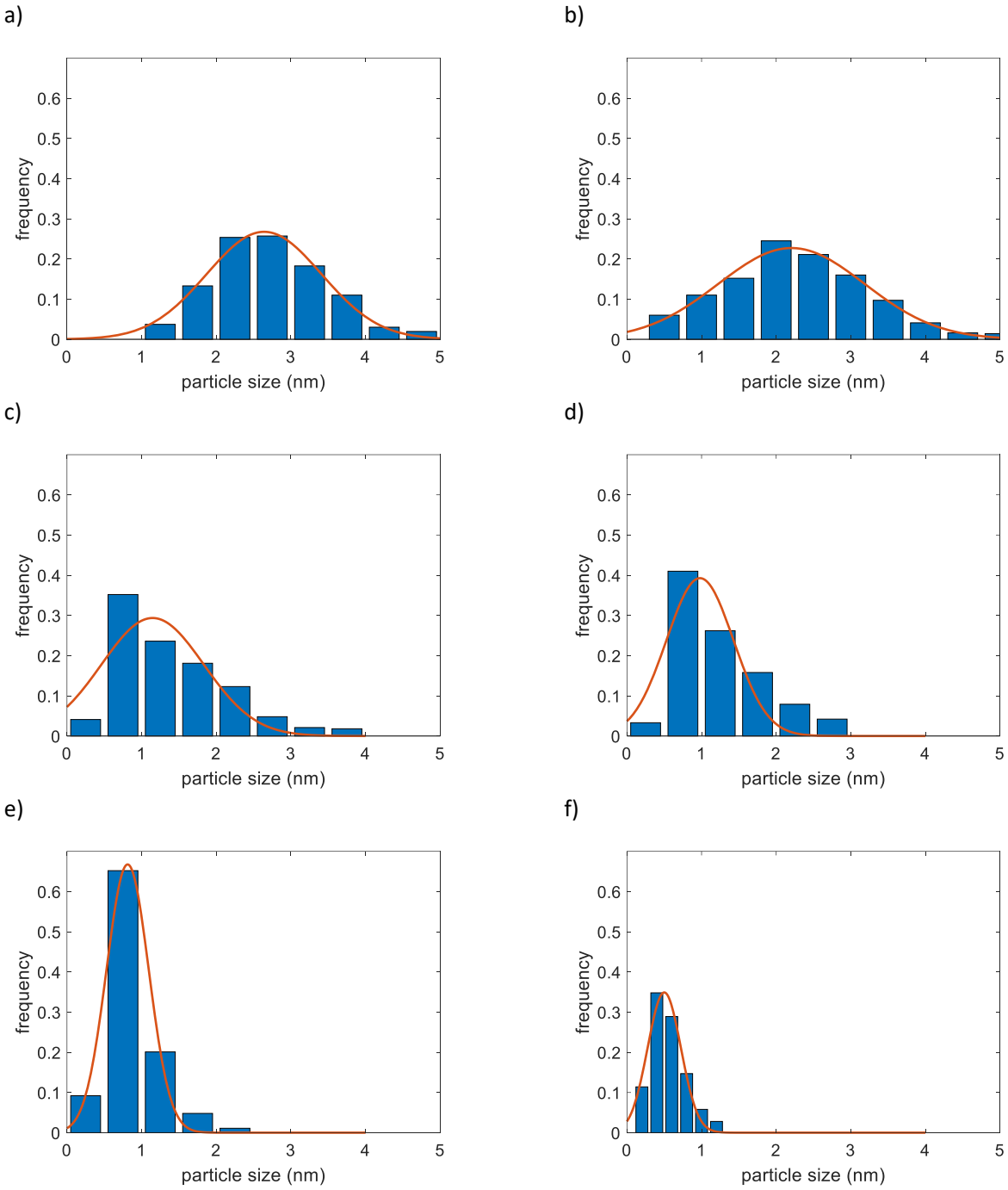

Fig. 3. Particle size distribution for the catalyst: a) Pd_{Escat}; b) Pd_2; c) Pd_{10}; d) Pd_{40}; e) Pd_{60}; and f) Pd_{200}. The orange lines are the Gaussian fits of the obtained distributions.

3.2. Catalytic studies

The catalytic performance of the reference PdEscat catalyst was evaluated in the reduction of AP in a stirred tank reactor. The absence of noticeable internal or external (Gas-Liquid or Liquid-Solid) mass transfer resistances has been checked (See supporting information S2), and the recovered data are consistent with intrinsic kinetics in chemical regime. In order to precisely study the behavior of the catalyst, the composition of the reaction as the function of time needs to be precisely determined. This could be done by ex-situ analysis by periodical liquid sampling for subsequent GC-FID analysis. Fig. 4a depicts a typical profile obtained according to this classical reaction progress monitoring. However, even if this procedure gives valuable results, the sampling frequency must be adapted to the activity of the studied catalyst. The hydrogen consumption evolution is another complementary data that can help study the catalyst's activity. This data is obtained indirectly by monitoring the H_2 pressure ($P_{H_2}^{res}$) and temperature (Tres) in the reservoir at a 1 Hz frequency. This monitoring was used to determine the corresponding H_2 uptake evolution by the reactive media (Fig. 4b). The hydrogen consumption was systematically checked to be in good agreement with the mass balance determined using GC/FID analysis of the reaction mixture.

Fig. 4a and 4b show that AP reacts through two successive reactions: hydrogenation of AP to the corresponding PE followed by hydrogenolytic rupture of the C–O bond, yielding EB (Fig. 1). Unlike experiments with Pd supported on various supports, no styrene was identified as intermediate under our conditions. This could be explained by the lower reaction temperature, 60°C vs. 130°C [20]. No hydrogenolysis reaction could be observed until an AP conversion higher than 80%. This could be explained by the stronger adsorption of AP on the active phase compared to PE. An apparent partial order in AP of zero for conversion up to 80% was observed (Fig. 4a). Then, the hydrogenolysis reaction started (Fig. 1), showing an apparent partial order in PE close to 1.

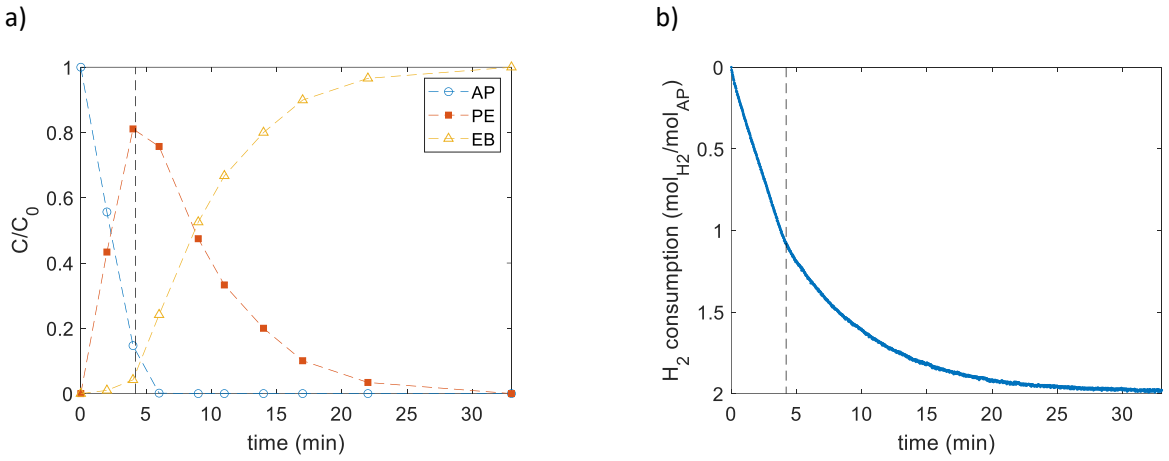

Fig. 4. a) Composition profile of the liquid phase; and b) corresponding H_2 reserve pressure consumption profile as the function of time during the hydrogenation of AP. Experimental conditions: 0.2 M AP in EtOH, 5 bar H_2, 60 °C, Pd_{Escat}, 0.2 mol% Pd.

3.3. Kinetic modeling

In the following, hydrogen uptake and liquid composition profiles will be used to precisely fit the kinetic constants of an appropriate model for these two reactions. This method appears interesting because a practical and quantitative catalyst activity comparison can be provided based on a limited set of kinetic parameters. Moreover, the modeling approach helps correctly handle catalyst activity when both reactions occur simultaneously, near the optimum.

Although most of the publications on AP reduction have focused on screening new catalysts and improving catalytic properties, only a few studies have addressed the development of kinetic models for this reaction [3,5,6,9,20]. Unfortunately, the experimental conditions used in these works (solvent, temperature, pressure) and the active metal used are different. Therefore, starting from these published data, a detailed set of experiments has been conducted on the Pd_{Escat} reference catalyst to select the most appropriate global kinetic description using the Langmuir-Hinshelwood-Hougen-Watson (LHHW) formalism. A wide experimental domain has been explored, including variations in the concentration (0.2 to 0.8 M) of starting reactant (AP), intermediate (PE), and final products (EB and water). The influence of H_2 pressure (2 to 15 bar) has also been experienced (see supporting information S3, Table S5). The best fit was obtained when considering the competitive adsorption of AP and PE associated with a non-competitive and dissociative adsorption for H_2 in the hydrogenation step. For the hydrogenolysis step, a non-dissociative H_2 activation and competitive adsorption between AP, PE, EB, and H_2 are required to represent the data well. This kinetic model is similar to the one derived in the work of Bergault *et al* [6] for a Rh/C catalyst. The corresponding kinetic rate expressions are given in equations (2) and (3), making use of 6 kinetic parameters (K_{AC}, K_{PE}, K_{EB}+K_{H_2O}, K_{H_2}, $k_{hydrogenation}$, and $k_{hydrogenolysis}$). Table 2 presents the values of the 6 regressed kinetic parameters in the case of this reference Pd_{Escat} catalyst, and Fig. S5 depicts the parity plots for liquid phase composition and H_2 uptake, demonstrating the excellent ability of the model to represent experimental data. Table S6 shows that the regressed parameters are not significantly correlated.

$$r_{hydrogenation}(t) = k_{hydrogenation} \cdot \frac{K_{AC}.C_{AC}(t)}{1+K_{AC}.C_{AC}(t)+K_{PE}.C_{PE}(t)} . \frac{(K_{H2}.P_{H2}(t))^{0.5}}{1+(K_{H2}.P_{H2}(t))^{0.5}} \quad (2)$$

$$r_{hydrogenolysis}(t) = k_{hydrogenolyse} \cdot \frac{K_{PE}.C_{PE}(t).K_{H2}.P_{H2}(t)}{(1+K_{AC}.C_{AC}(t)+K_{PE}.C_{PE}(t)+(K_{EB}+K_{H2O}).C_{EB}(t)+K_{H2}.P_{H2}(t))^2} \quad (3)$$

Table 4.

Optimized parameters of the LHHW kinetic model applied to the Pd_{Escat} reference catalyst with 95% confidence intervals.

K_{AC}	K_{PE}	K_{EB}+K_{H_2O}	K_{H_2}	$k_{hydrogenation}$	$k_{hydrogenolysis}$
$L \cdot mol^{-1}$	$L.mol^{-1}$	$L.mol^{-1}$	bar^{-1}	$mol.h^{-1}.mol_{surface\ Pd}^{-1}$	$mol.h^{-1}.mol_{surface\ Pd}^{-1}$
139 ± 9	9.0 ± 0.5	9.6 ± 0.6	0.54 ± 0.02	31600 ± 400	$82000 \cdot \pm 2000$

A similar experiment has been repeated for the different catalysts of this study with the following conditions: 0.2M AP in ethanol; 60 °C; 5 bar; Pd 0.03 mol%. The evolution of the liquid phase composition is presented in Fig. 5 a-e. Similar behaviors to the Pd_{Escat} catalyst are observed, with pseudo-zeroth order for the hydrogenation step and pseudo-first order for the hydrogenolysis one. Furthermore, noticeable differences in activity and selectivity near the optima in PE are present when the SA/NP ratio is changed.

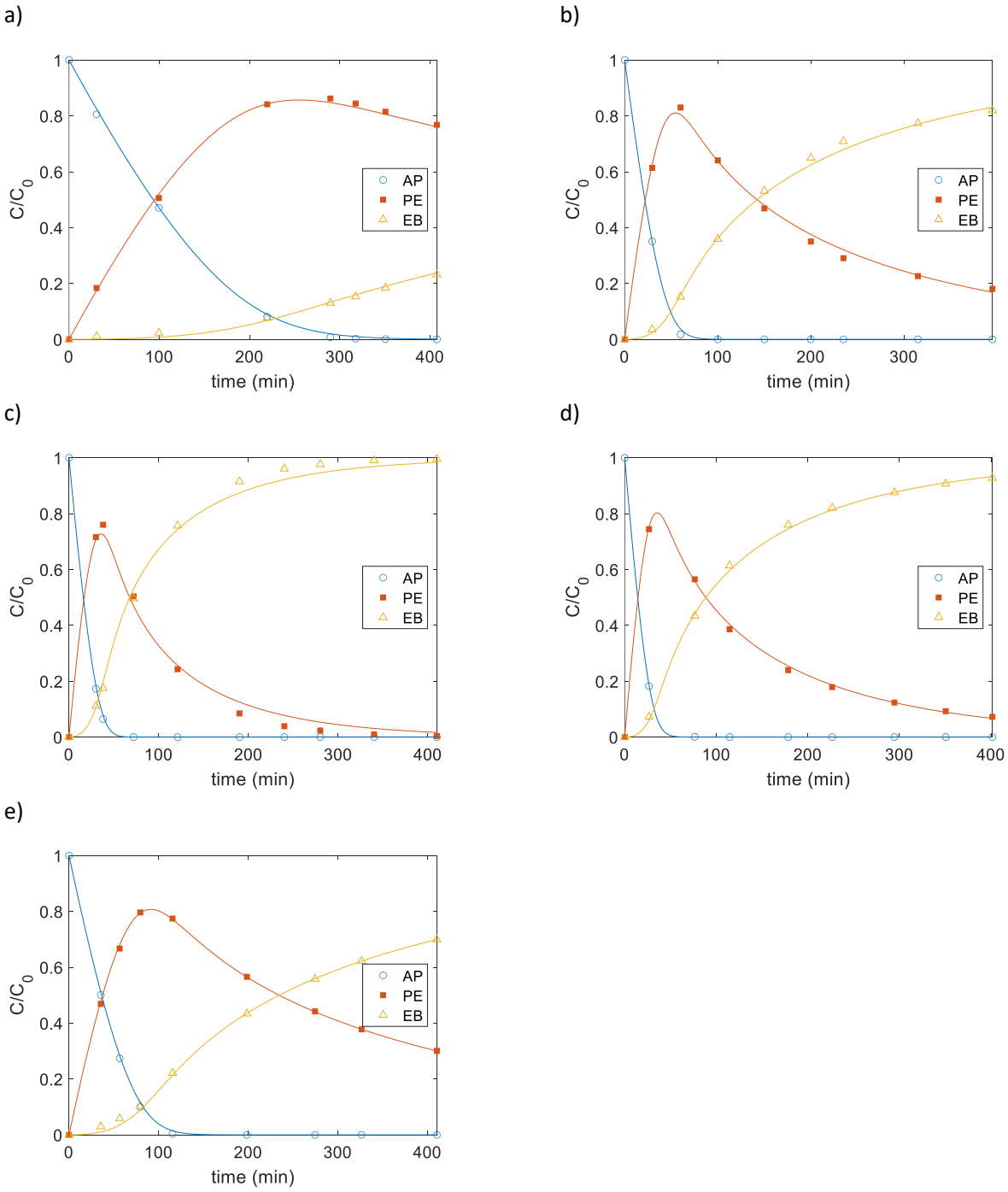

Fig. 5. Liquid phase composition evolution with time for the different catalysts of this study: a) Pd_{200}; b) Pd_{60}; c) Pd_{40}; d) Pd_{10}, and e) Pd_2. Characteristics of the Pd catalysts are listed in table 1. The lines are the results of the model fittings. Experimental conditions: 0.2M AP in EtOH, 60°C, 5 bars H_2, Pd 0.03 mol%.

3.4. Impact of the SA/NP ratio on the kinetics

To practically and quantitatively determine the impact of the SA/NP ratio and, thus the impact of the surface Pd distribution between SA and NP on the observed kinetics, the previous model developed for the Pd_{Escat} catalyst has been adjusted for each catalyst of this series. Because of a limited set of experimental data, the regression was reasonably limited to 4 parameters: $k_{hydrogenation}$, $k_{hydrogenolysis}$, and product adsorption parameters (K_{PE} and K_{EB}+K_{H2O}), while reactant adsorption parameters (K_{AP} and K_{H2} determined previously for the Pd_{Escat} catalyst) have been assumed constant. This limited fitting allows a low correlation between the regressed parameters (Table S7) and a good fit of a limited data set. The continuous lines in Fig. 5a-e are the results of these fittings.

Fig. 6 presents the parity plot obtained for all the liquid composition profiles for all these catalysts. It confirms the excellent ability of this modeling approach to represent the experimental data. It is noteworthy that this is a first approach to quantify the impact of the SA/NP ratio on the kinetic of these reactions. A micro-kinetic approach considering the different types of sites, Pd SA and Pd NP, and the hydrogen spillover step would be of greater interest but cannot yet be implemented and would require very specific experiments that are not the object of this work.

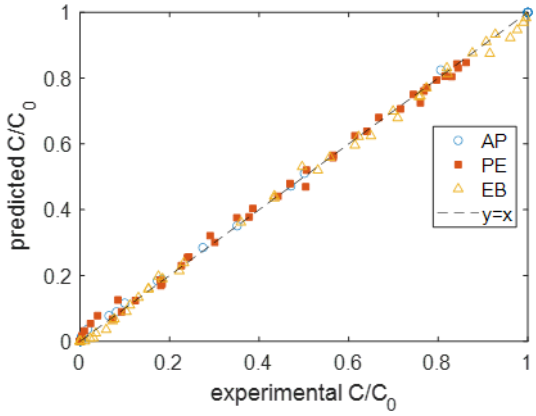

Fig. 6. Parity plot showing the experimental composition of the liquid phase vs. predicted concentration for the Pd/CNT series. Experimental conditions: 0.2M AP in EtOH, 60°C, 5 bars H_2, Pd 0.03 mol%.

Table 3 presents the results of the regressed parameters. They allow for quantitatively discussing the impact of the distribution of Pd between SA and NP on the observed catalyst activity and selectivity. Fig. 7 depicts these different kinetic constants graphically as the function of the atomic fraction of SA relative to the total surface atom of Pd.

Table 3.

Optimized parameters of the LHHW kinetic model applied to the different Pd/CNT catalysts with 95% confidence intervals.

Catalyst	K_{AC}	K_{PE}	$K_{EB}+K_{H2O}$	K_{H2}	$k_{hydrogenation}$	$k_{hydrogenolysis}$
	$L \cdot mol^{-1}$	$L.mol^{-1}$	$L.mol^{-1}$	bar^{-1}	$mol.h^{-1}.mol_{surface\ Pd}^{-1}$	$mol.h^{-1}.mol_{surface\ Pd}^{-1}$
Pd_2					6400 ± 200	9900 ± 400
Pd_{10}					14200 ± 900	23000 ± 2000
Pd_{40}	139 ± 9	33 ± 7	75 ± 9	0.54 ± 0.02	10500 ± 700	32000 ± 3000
Pd_{60}					8000 ± 500	12000 ± 1000
Pd_{200}					1900 ± 100	1700 ± 200

Significant variations of the activities of the catalysts are observed and quantified for the 2 considered reactions and these 5 different SA/NP ratios. The non-linear behavior observed when varying the distribution of Pd between SA and NP confirms the cooperative effects of SA and NP already stated (but not quantified) in the literature [41]. This effect is quantified here, and the concept is extended to the second consecutive reaction. Moreover, the present study clearly demonstrates that the presence of SA in the catalyst is insufficient to obtain higher catalytic performance, but it is crucial to control the ratio between SA and NP to obtain optimal catalytic activity. When considering the hydrogenation step, moving from a ratio of 2 (catalyst with a significant number of NP) to a ratio of 10 implies a twofold increase in the kinetic constant, confirming the critical role of this parameter in obtaining very cooperative active catalysts.

Interestingly, different optimal ratios are reached for the two consecutive reactions (Fig. 7). An optimal ratio of 10 (corresponding to an atomic fraction of Pd in the SA of 17%) is obtained for the hydrogenation of AP. An optimal ratio close to 40 (corresponding to an atomic fraction of Pd in the SA of 58%) for the hydrogenolysis of PE (Fig. 7). These values are probably correlated to the nature of the support and its ability to promote hydrogen spillover [37,44,45]. The justifications for the optimal value of this Pd SA/NP ratio are still unclear and will be further investigated in a separate work. Micro-kinetics data and mechanistic insights from DFT calculations should be necessary to understand the contribution of Pd SA and Pd NP, as well as the influence of the hydrogen spillover on the reduction of carbonyls. Finally, as expected, moving to very high values of atomic fraction of SA, the catalytic activities decrease for both reactions, confirming the tendencies observed in the literature for catalysts containing mainly single atoms [29,30,36].

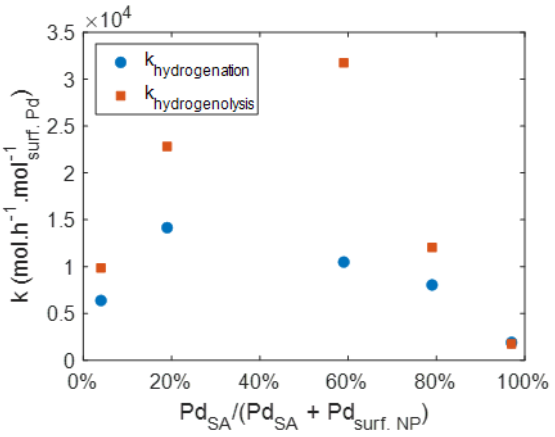

Fig. 7. Kinetic constants for the hydrogenation of AP to PE and for the hydrogenolysis of PE to EB as a function of the atomic fraction of SA for the Pd/CNT series. Experimental conditions: 0.2M AP in EtOH, 60°C, 5 bars H_2, Pd 0.03 mol%.

Fig. 8a shows the profiles of PE selectivity as the function of AP conversion. As expected, the selectivity toward PE remains the highest at high conversion for the catalyst Pd_{200}, having the highest fraction of Pd in the SA form (> 95%). The lowest selectivity-conversion profile is observed for the catalyst Pd_{40}. These results are in good agreement with Fig. 8b, which depicts the ratio between hydrogenation and hydrogenolysis kinetic parameters as a function of the atomic fraction of surface Pd in the form of SA for the different Pd/CNT catalysts. It indicates a good ability of the global modeling approach to handle and quantify the differences observed between catalysts near the optimum.

a)

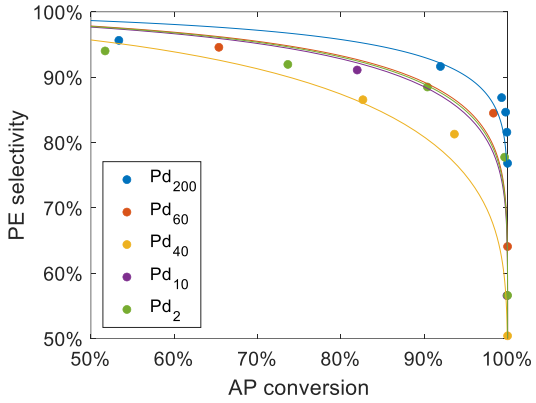

b)

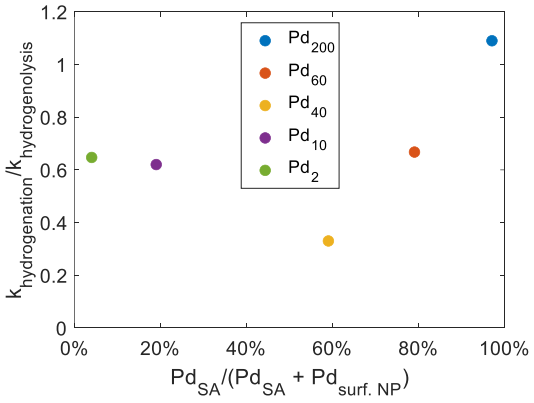

Fig. 8. a) Selectivity toward PE as the function of AP conversion for the Pd/CNT series. Characteristics of the Pd catalysts are listed in table 1. The lines are the results of the model fittings. b) Ratio between hydrogenation and hydrogenolysis fitted kinetic parameters as the function of the atomic fraction of Pd present in the SA. Experimental conditions: 0.2M AP in EtOH, 60 °C, 5 bars H_2, Pd 0.03 mol%.

4. Conclusion

Well-defined Pd catalysts supported on CNT with a controlled SA/NP ratio were evaluated for the reduction of acetophenone. This study demonstrates that the kinetic constants of the reduction to phenyl ethanol and further hydrogenolysis to ethyl benzene are largely impacted by the SA/NP ratio of the catalysts. This result could be linked to the cooperativity between the two kinds of active sites thanks to hydrogen spillover on the functionalized CNT support. Additionally, the optimum ratio changed for the two hydrogenation and hydrogenolysis steps. Such a controlled active phase tuning is expected to pave the way to very efficient catalysts involving supported metal single atoms. A thorough study of the theoretical mechanism of acetophenone hydrogenation is in progress to discuss further the possible micro-mechanism involved. In addition, the presence of clusters and cluster size impact on the catalytic performance should be further studied.

CRediT authorship contribution statement

Vincent Bernardin: Investigation, Methodology, Data curation, Visualization. Laurent Vanoye: Methodology, Data curation, Visualization. Camila Rivera-Cárcamo: Investigation, Catalysts synthesis and characterization. Philippe Serp: Resources, Project administration, Methodology, Writing – review & editing. Alain Favre-Réguillon: Methodology, Supervision, Writing – review & editing. Régis Philippe: Resources, Project administration, Methodology, Supervision, Visualization, Writing - Review & Editing.

Declaration of Competing Interest

The authors declare that they have no known competing financial interests or personal relationships that could have appeared to influence the work reported in this paper.

Data Availability

Data will be made available on request.

Acknowledgments

This work was supported by the French "Agence Nationale de la Recherche" (project ANR-19-CE07-0030, COMET), which is gratefully acknowledged. Frédéric Bornette is acknowledged for contributing to the experimental setup and the development of the acquisition tools.

References

[1] D.C. Costa, J.F. Bengoa, S.G. Marchetti, V. Vetere, Impact of the surface hydrophobicity/hydrophilicity ratio on the catalytic properties of Ni nanoparticles/MCM-41 system used in the hydrogenation of acetophenone, Catal. Today, 372 (2021) 20-26.

[2] Y. Gou, X. Liang, B. Chen, Catalytic hydrogenation of acetophenone over shape controlled Pd catalysts supported on sheet-like NiO, Catal. Today, 216 (2013) 200-204.

[3] M.V. Rajashekharam, I. Bergault, P. Fouilloux, D. Schweich, H. Delmas, R.V. Chaudhari, Hydrogenation of acetophenone using a 10% Ni supported on zeolite Y catalyst: kinetics and reaction mechanism, Catal. Today, 48 (1999) 83-92.

[4] B. Wang, M. Jin, H. An, Z. Guo, Z. Lv, Hydrogenation Performance of Acetophenone to 1-Phenylethanol on Highly Active Nano Cu/SiO_2 Catalyst, Catal. Lett., 150 (2019) 56-64.

[5] S. Lee, Z. Yu, N. Zaborenko, A. Varma, Acetophenone hydrogenation on Rh/Al_2O_3 catalyst: Intrinsic reaction kinetics and effects of internal diffusion, Chem. Eng. J., 288 (2016) 711-723.

[6] I. Bergault, P. Fouilloux, C. Joly-Vuillemin, H. Delmas, Kinetics and intraparticle diffusion modelling of a complex multistep reaction: Hydrogenation of acetophenone over a rhodium catalyst, J. Catal., 175 (1998) 328-337.

[7] M. Chen, N. Maeda, A. Baiker, J. Huang, Molecular Insight into Pt-Catalyzed Chemoselective Hydrogenation of an Aromatic Ketone by In Situ Modulation–Excitation IR Spectroscopy, ACS Catal., 2 (2012) 2007-2013.

[8] C.-S. Chen, H.-W. Chen, W.-H. Cheng, Study of selective hydrogenation of acetophenone on Pt/SiO_2, Appl. Catal., A, 248 (2003) 117-128.

[9] F. Gao, A.D. Allian, H. Zhang, S. Cheng, M. Garland, Chemical and kinetic study of acetophenone hydrogenation over Pt/Al_2O_3: Application of BTEM and other multivariate techniques to quantitative on-line FTIR measurements, J. Catal., 241 (2006) 189-199.

[10] R. Paul, S.C. Shit, T. Fovanna, D. Ferri, B. Srinivasa Rao, G. Gunasooriya, D.Q. Dao, Q.V. Le, I. Shown, M.P. Sherburne, Q.T. Trinh, J. Mondal, Realizing Catalytic Acetophenone Hydrodeoxygenation with Palladium-Equipped Porous Organic Polymers, ACS Appl. Mater. Interfaces, 12 (2020) 50550-50565.

[11] C. Sumner, W. Burchett, Developments in the Pd Catalyzed Hydrogenation of Oxygenated Organic Compounds, Top. Catal., 55 (2012) 480-485.

[12] Y.-Z. Xiang, Y.-A. Lv, T.-Y. Xu, X.-N. Li, J.-G. Wang, Selectivity difference between hydrogenation of acetophenone over CNTs and ACs supported Pd catalysts, J. Mol. Catal. A: Chem., 351 (2011) 70-75.

[13] M. Chen, N. Maeda, A. Baiker, J. Huang, Hydrogenation of Acetophenone on Pd/Silica–Alumina Catalysts with Tunable Acidity: Mechanistic Insight by In Situ ATR-IR Spectroscopy, ACS Catal., 8 (2018) 6594-6600.

[14] K.D. Kim, Z. Wang, Y. Tao, H. Ling, Y. Yuan, C. Zhou, Z. Liu, M. Gaborieau, J. Huang, A. Yu, The Comparative Effect of Particle Size and Support Acidity on Hydrogenation of Aromatic Ketones, ChemCatChem, 11 (2019) 4810-4817.

[15] W. Alsalahi, W. Tylus, A.M. Trzeciak, Highly selective hydrogenation of aromatic ketones to alcohols in water: effect of PdO and ZrO_2, Dalton Trans, 50 (2021) 10386-10393.

[16] Z. Wang, S. Pokhrel, M. Chen, M. Hunger, L. Mädler, J. Huang, Palladium-doped silica–alumina catalysts obtained from double-flame FSP for chemoselective hydrogenation of the model aromatic ketone acetophenone, J. Catal., 302 (2013) 10-19.

[17] Y. Zhang, S. Zhan, K. Liu, M. Qiao, N. Liu, R. Qin, L. Xiao, P. You, W. Jing, N. Zheng, Heterogeneous Hydrogenation with Hydrogen Spillover Enabled by Nitrogen Vacancies on Boron Nitride-Supported Pd Nanoparticles, Angew. Chem. Int. Ed., (2023) e202217191.

[18] S.R. More, G.D. Yadav, Effect of Supercritical CO2 as Reaction Medium for Selective Hydrogenation of Acetophenone to 1-Phenylethanol, ACS Omega, 3 (2018) 7124-7132.

[19] C.-S. Chen, H.-W. Chen, Enhanced selectivity and formation of ethylbenzene for acetophenone hydrogenation by adsorbed oxygen on Pd/SiO_2, Appl. Catal., A, 260 (2004) 207-213.

[20] M. Bejblová, P. Zámostný, L. Červený, J. Čejka, Hydrogenation and hydrogenolysis of acetophenone, Collect. Czech. Chem. Commun., 68 (2003) 1969-1984.

[21] R. Paul, S.C. Shit, T. Fovanna, D. Ferri, B. Srinivasa Rao, G.T.K.K. Gunasooriya, D.Q. Dao, Q.V. Le, I. Shown, M.P. Sherburne, Q.T. Trinh, J. Mondal, Realizing Catalytic Acetophenone Hydrodeoxygenation with Palladium-Equipped Porous Organic Polymers, ACS Appl. Mater. Interfaces, 12 (2020) 50550-50565.

[22] A. Wang, J. Li, T. Zhang, Heterogeneous single-atom catalysis, Nat. Rev. Chem., 2 (2018) 65-81.

[23] S. Liang, C. Hao, Y. Shi, The Power of Single-Atom Catalysis, ChemCatChem, 7 (2015) 2559-2567.

[24] Z.-Y. Li, Z. Yuan, X.-N. Li, Y.-X. Zhao, S.-G. He, CO Oxidation Catalyzed by Single Gold Atoms Supported on Aluminum Oxide Clusters, J. Am. Chem. Soc., 136 (2014) 14307-14313.

[25] L. Sun, J. Xu, X. Liu, B. Qiao, L. Li, Y. Ren, Q. Wan, J. Lin, S. Lin, X. Wang, H. Guo, T. Zhang, High-Efficiency Water Gas Shift Reaction Catalysis on α-MoC Promoted by Single-Atom Ir Species, ACS Catal., 11 (2021) 5942-5950.

[26] S. Tao, D. Yang, M. Wang, G. Sun, G. Xiong, W. Gao, Y. Zhang, Y. Pan, Single-atom catalysts for hydroformylation of olefins, iScience, 26 (2023) 106183.

[27] Q. Zhang, J. Guan, Single-Atom Catalysts for Electrocatalytic Applications, Adv. Funct. Mater., 30 (2020) 2000768.

[28] L. Zhang, M. Zhou, A. Wang, T. Zhang, Selective Hydrogenation over Supported Metal Catalysts: From Nanoparticles to Single Atoms, Chem. Rev., 120 (2020) 683-733.

[29] M.D. Rossell, F.J. Caparrós, I. Angurell, G. Muller, J. Llorca, M. Seco, O. Rossell, Magnetite-supported palladium single-atoms do not catalyse the hydrogenation of alkenes but small clusters do, Catal. Sci. Technol., 6 (2016) 4081-4085.

[30] J. Yang, X. Du, B. Qiao, Comprehensive activity evaluation of single-atom catalysts, Chem Catalysis, 3 (2023) 100424.

[31] S. Büchele, Z. Chen, S. Mitchell, R. Hauert, F. Krumeich, J. Pérez-Ramírez, Tailoring Nitrogen-Doped Carbons as Hosts for Single-Atom Catalysts, ChemCatChem, 11 (2019) 2812-2820.

[32] Y. Liu, B. Wang, Q. Fu, W. Liu, Y. Wang, L. Gu, D. Wang, Y. Li, Polyoxometalate-Based Metal–Organic Framework as Molecular Sieve for Highly Selective Semi-Hydrogenation of Acetylene on Isolated Single Pd Atom Sites, Angew. Chem. Int. Ed., 60 (2021) 22522-22528.

[33] X. Tao, B. Nan, Y. Li, M. Du, L.-l. Guo, C. Tian, L. Jiang, L. Shen, N. Sun, L.-N. Li, Highly Active Isolated Single-Atom Pd Catalyst Supported on Layered MgO for Semihydrogenation of Acetylene, ACS Appl. Energy Mater., 5 (2022) 10385-10390.

[34] X. Huang, H. Yan, L. Huang, X. Zhang, Y. Lin, J. Li, Y. Xia, Y. Ma, Z. Sun, S. Wei, J. Lu, Toward Understanding of the Support Effect on Pd_1 Single-Atom-Catalyzed Hydrogenation Reactions, J. Phys. Chem. C, 123 (2019) 7922-7930.

[35] H. Yan, H. Cheng, H. Yi, Y. Lin, T. Yao, C. Wang, J. Li, S. Wei, J. Lu, Single-Atom Pd_1/Graphene Catalyst Achieved by Atomic Layer Deposition: Remarkable Performance in Selective Hydrogenation of 1,3-Butadiene, J. Am. Chem. Soc., 137 (2015) 10484-10487.

[36] C. Rivera-Cárcamo, I.C. Gerber, I. del Rosal, B. Guicheret, R. Castro Contreras, L. Vanoye, A. Favre-Réguillon, B.F. Machado, J. Audevard, C. de Bellefon, R. Philippe, P. Serp, Control of the single atom/nanoparticle ratio in Pd/C catalysts to optimize the cooperative hydrogenation of alkenes, Catal. Sci. Technol., 11 (2021) 984-999.

[37] P. Serp, Cooperativity in supported metal single atom catalysis, Nanoscale, 13 (2021) 5985-6004.

[38] W. Gao, S. Liu, G., Sun, C. Zhang, Y. Pan, Single-Atom Catalysts for Hydrogen Activation. Small 2023, 2300956.

[39] C. Chu, D. Huang, S. Gupta, S. Weon, J. Niu, E. Stavitski, C. Muhich, J.-H. Kim, Neighboring Pd single atoms surpass isolated single atoms for selective hydrodehalogenation catalysis, Nat. Commun., 12 (2021) 5179.

[40] U. Petek, F. Ruiz-Zepeda, M. Bele, M. Gaberšček, Nanoparticles and Single Atoms in Commercial Carbon-Supported Platinum-Group Metal Catalysts, Catalysts, 9 (2019) 134.

[41] L. Kuai, Z. Chen, S. Liu, E. Kan, N. Yu, Y. Ren, C. Fang, X. Li, Y. Li, B. Geng, Titania supported synergistic palladium single atoms and nanoparticles for room temperature ketone and aldehydes hydrogenation, Nat. Commun., 11 (2020) 48.

[42] J. Yang, L. Yang, L. Zhang, T. Yu, D. Zhai, H. Wang, W. Zhou, Y. Li, G. Ren, L. Sun, W. Deng, Hydrogenation Reactions with Synergistic Catalysis of Pd single atoms and nanoparticles under Near-Ambient Conditions, Chem. Eur. J., (2022) e202203108.

[43] R. Prins, Hydrogen Spillover. Facts and Fiction, Chem. Rev., 112 (2012) 2714-2738.

[44] L. Warczinski, C. Hättig, How Nitrogen Doping Affects Hydrogen Spillover on Carbon-Supported Pd Nanoparticles: New Insights from DFT, J. Phys. Chem. C, 125 (2021) 9020-9031.

[45] I.C. Gerber, P. Serp, A Theory/Experience Description of Support Effects in Carbon-Supported Catalysts, Chem. Rev., 120 (2020) 1250-1349.

[46] R.C. Contreras, B. Guicheret, B.F. Machado, C. Rivera-Cárcamo, M.A. Curiel Alvarez, B. Valdez Salas, M. Ruttert, T. Placke, A. Favre-Réguillon, L. Vanoye, C. de Bellefon, R. Philippe, P. Serp, Effect of mesoporous carbon support nature and pretreatments on palladium loading, dispersion and apparent catalytic activity in hydrogenation of myrcene, J. Catal., 372 (2019) 226-244.

[47] L. Vanoye, B. Guicheret, C. Rivera-Carcamo, R.C. Contreras, C. de Bellefon, V. Meille, P. Serp, R. Philippe, A. Favre-Reguillon, Process intensification of the catalytic hydrogenation of squalene using a Pd/CNT catalyst combining nanoparticles and single atoms in a continuous flow reactor, Chem. Eng. J., 441 (2022) 135951.

[48] B. Guicheret, L. Vanoye, C. Rivera-Carcamo, C. de Bellefon, P. Serp, R. Philippe, A. Favre-Reguillon, Solvent-Free Hydrogenation of Squalene Using Parts per Million Levels of Palladium Supported on Carbon Nanotubes: Shift from Batch Reactor to Continuous-Flow System, ChemSusChem, 15 (2022) e202200916.

[49] C.-T. Kuo, Y. Lu, L. Kovarik, M. Engelhard, A.M. Karim, Structure Sensitivity of Acetylene Semi-Hydrogenation on Pt Single Atoms and Subnanometer Clusters, ACS Catal., 9 (2019) 11030-11041.

[50] A. Borodziński, M. Bonarowska, Relation between Crystallite Size and Dispersion on Supported Metal Catalysts, Langmuir, 13 (1997) 5613-5620.

Supporting information

Acetophenone hydrogenation and hydrogenolysis with Pd/CNT catalysts: Highlighting the Synergy between Single Atoms and Nanoparticles by Kinetic modeling

Vincent Bernardin,[1] Laurent Vanoye,[1] Camila Rivera-Cárcamo,[2] Philippe Serp,[2*] Alain Favre-Réguillon[1,3*], Régis Philippe[1*]

S1. XPS characterization of the catalysts

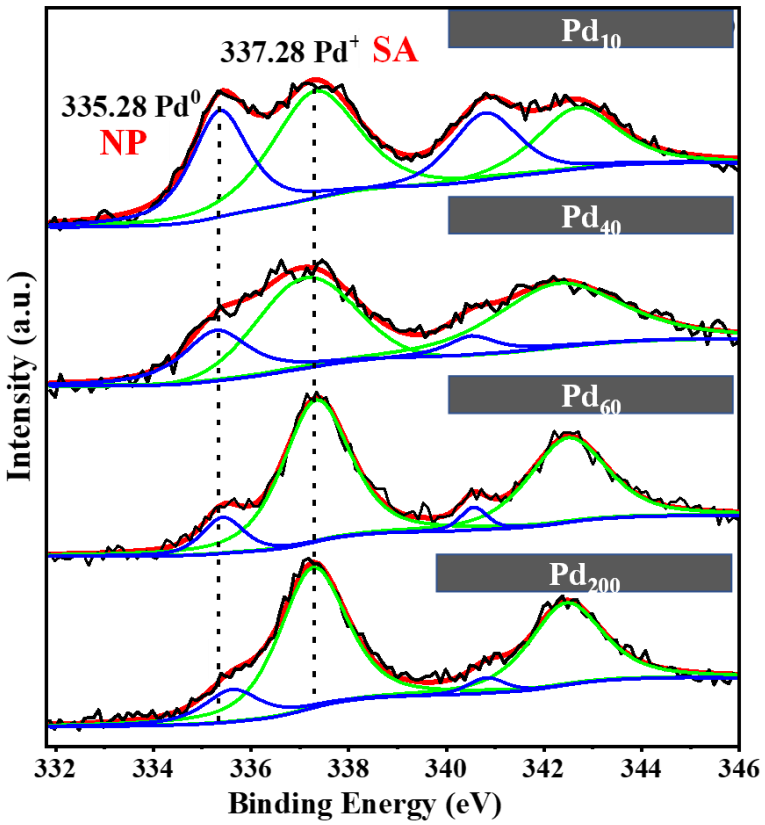

Figure S 1. XPS spectra of Pd_{200}, Pd_{60}, Pd_{40} and Pd_{10} samples.

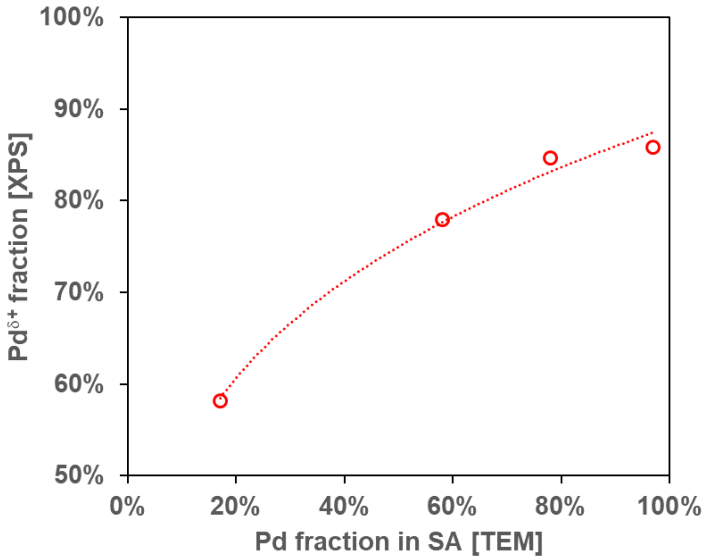

Figure S 2. Correlation between the fractions of SA measured by STEM and the $Pd^{\delta+}$fraction determined from XPS

S2. Evaluation of possible mass transfer resistances

S2.1. Physico-chemical properties

Table S 1 lists all the physicochemical properties considered in our mass transfer calculations. These properties are quite common and come from the literature or measurements.

Table S 1

Properties used for mass transfer assessment calculations. (*: measured experimentally)

Component	Property	Symbol	Value
Liquid Ethanol	Viscosity (Pa.s)	μ_L	$6.0.10^{-2}$
	surface tension ($N.m^{-1}$)	σ_L	$1.9.10^{-2}$
	Density ($kg.m^{-3}$)	ρ_L	770
	H_2 diffusivity ($m^2.h^{-1}$)	$D_{m,\,H2}$	$7.20.10^{-6}$
	H_2 solubility ($mol.m^{-3}$)*	C^{sat}_{H2}	14.6
Gaseous hydrogen	Viscosity (Pa.s)	μ_G	$1.07.10^{-5}$
	Density ($kg.m^{-3}$)	ρ_G	1.22
CNT support	Skeleton density ($kg.m^{-3}_{skeleton}$)	ρ_s	1900
	Dry particle density ($kg.m^{-3}_{particle}$)	ρ_p	600
	Wetted particle density ($kg.m^{-3}_{particle}$)	ρ_p	1100
	Average particle diameter (µm)	d_p	2
	Internal porosity ($m^3_{void}.m^{-3}_{particle}$)	β	70%
	Tortuosity (-)	τ	≈1
Activated carbon support	Skeleton density ($kg.m^{-3}_{skeleton}$)	ρ_s	1900
	Dry particle density ($kg.m^{-3}_{particle}$)	ρ_p	760
	Wetted particle density ($kg.m^{-3}_{particle}$)	ρ_p	1200
	Average particle diameter (µm)	d_p	25
	Internal porosity ($m^3_{void}.m^{-3}_{particle}$)	β	60%
	Tortuosity (-)	τ	3

S2.2. Gas-Liquid external mass transfer

The mass transfer coefficient $k_L.a_{G\text{-}L}$ and hydrogen solubility in 0.2 M AP in ethanol have been measured experimentally using a physical absorption technique [1,2] in the same experimental conditions than the one used for AP hydrogenation, but without catalyst (60°C, 5bar H_2, 1200 rpm stirring). The H_2 consumption profile of the reserve (Figure S1) allowed adjusting and recovering these 2 parameters of the system thanks to the mass balance derived in equations S1 to S3: the mass transfer coefficient $k_L.a_{G\text{-}L}$ and the final saturation C^{sat}_{H2}. Values of 1100 h^{-1} (0.31 s^{-1}) and 14.6 $mol.m^{-3}$ are obtained for $k_La_{G\text{-}L}$ and the hydrogen solubility, respectively.

$$dn^L_{H2}(t) = -dn^{res}_{H2}(t) = -dP^{res}(t)\frac{V_{res}}{RT_{res}} \quad \text{(Eq. S1)}$$

$$k_L a_{G-L} V_R \left(C^{sat}_{H2} - C^L_{H2}(t)\right) = \frac{dn^L_{H2}(t)}{dt} = V_L \frac{dC^L_{H2}(t)}{dt} \quad \text{(Eq. S2)}$$

$$-dP^{res}(t) = \frac{RT^{res}}{V_{res}} C^{sat}_{H2} V_L \left(1 - \exp\left(\frac{k_L a_{G-L}}{\varepsilon_L} t\right)\right) \quad \text{(Eq. S3)}$$

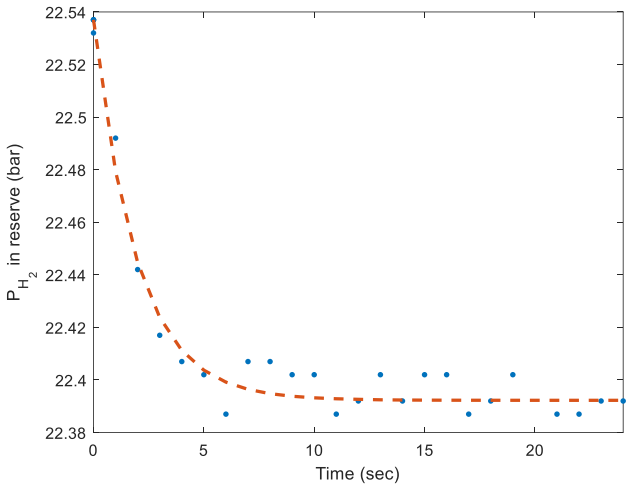

Figure S 3. Evolution of H_2 pressure in the gas reserve to assess mass transfer capabilities of the reactor. Experimental points are the blue dots and the fit of eq. S3 is given by the red dotted line.

Using these data, a theoretical maximum H_2 consumption molar flowrate F^{G-L}_{max} (as defined in equation S4) can be calculated to a value of 3.2 $mol.h^{-1}$. Then, it can be used to define the corresponding maximum theoretical apparent reaction rate in the G-L mass transfer regime (equation S5). Here it corresponds to a value of $2.7.10^4\ mol_{H_2}.h^{-1}.m_L^{-3}$.

$$F^{G-L}_{max} = k_L.a_{G-L}.V_R.C^{sat}_{H_2} \qquad \left(mol_{H_2}.h^{-1}\right) \quad \text{(Eq. S4)}$$

$$\overline{r_{H_2}^{max,G-L}} = \frac{F_{max}^{G-L}}{V_L} \qquad \left(mol_{H_2}.h^{-1}.m_L^{-3}\right) \quad \text{(Eq. S5)}$$

This value can be compared to the maximal apparent consumption rate, $\overline{r_{H_2}^{max,exp}}$ (expressed in the same units, $mol_{H2}.h^{-1}.m_L^{-3}$), determined experimentally from H_2 monitoring from the reserve. This non-dimensional ratio is equivalent to an external fraction related to the G-L mass transfer limitation, $f^{G\text{-}L}_{ex}$, defined in equation S6.

$$f_{ex}^{G-L} = \left(\frac{C_{H2}^{sat} - C_{H2}^{L}(t)}{C_{H2}^{sat}}\right) = \frac{\overline{r_{H_2}^{max,exp}}}{\overline{r_{H_2}^{max,G-L}}} \qquad \text{(Eq. S6)}$$

For all the experiments of this study, these criteria are found to be lower than 5%, thus indicating the absence of G-L mass transfer limitation. The highest apparent reaction rate observed was $3.7.10^3$ $mol.h^{-1}.m^3_L$ (60°C, 5 bar H_2, 0.2M AP in ethanol, and 0.2 mol% Pd_{Escat}) for the experiment with the most significant quantity of catalyst. Even with this point, the f_{ex}^{G-L} value reaches only 14%, which remains satisfactory for discussing intrinsic kinetics.

Moreover, knowing that in such reactive catalyst slurries, G-L mass transfer accelerations are likely [3,4], one can expect that the true experimental maximum reaction rate reachable in reactive conditions is significantly increased (see equation S7), leading to a less important effective resistance. This phenomenon is well known and explained by the presence of fine solid catalyst particles in the liquid boundary layer near the interface.

$$F_{max}^{G-L} = Ek_L.a_{G-L}.V_R.C_{H_2}^{sat} \qquad \left(mol_{H_2}.h^{-1}\right) \text{(Eq. S7)}$$

To further validate the absence of G-L mass transfer limitation, the solid catalyst content has been increased, and the observed reaction rate (in $mol_{H2}.h^{-1}.L_{liq.}^{-1}$) appears directly proportional to the solid catalyst content, thus confirming the absence of G-L mass transfer limitations, even for the most demanding conditions experienced.

S2.3. Liquid-solid external mass transfer

In G-L-S slurry reactors, L-S external mass transfer is often less limiting than the G-L one. The classical external mass transfer fraction fL-Sex, defined in equation (S8), has been used to verify this common assumption. In this equation, $\overline{r_{p,H_2}}$ is the apparent reaction rate (expressed in $mol_{H2}.m_{cata}^{-3}.s^{-1}$); L is the characteristic length of the catalyst ($V_p/S_P=d_p/6$ for spherical particles, expressed in m), and k_S is the L-S mass transfer coefficient (expressed in $m.s^{-1}$). The mass transfer coefficient has been estimated using the well-known correlation of Armenante & Kirwan [1] for solid catalysts in slurries (Equation S8).

$$f_{ex}^{L-S} = \frac{\overline{r_{p,H_2}}.L}{k_S.C_{H_2}^{sat}} \qquad \text{(Eq. S8)}$$

Table S 2 shows that the estimated values of f^{L-S}_{ex} are, in any case, far below 5%, thus leading to negligible mass transfer resistance, as expected.

Table S 2
Appraisal of possible L-S external mass transfer limitations.

Catalyst	f^{L-S}_{ex}
Pd_2	0.001%
Pd_{10}	0.003%
Pd_{40}	0.003%
Pd_{60}	0.002%
Pd_{200}	0.000%
Pd_{Escat}	0.207%

S2.4. Internal mass transfer

The classical Weisz-Prater criterion [5] ϕ' has been used to evaluate a possible internal mass transfer limitation. Its formula is given in equation S9. When the criterion is inferior to 1, a surface efficiency η_{su} of 1 is stated. When superior to 1, a surface efficiency is approximated as 1/ϕ', as recalled in equation S10.

$$\varphi' = \frac{\overline{r_{p,H_2}}.L^2}{D_{H2}^{eff}.C_{H2}^{su}} \quad with\ D_{H2}^{eff} = \frac{\beta_p}{\tau_p}.D_{H2}^{m} \qquad \text{(Eq. S9)}$$

$$\begin{cases} \eta_{su} \approx 1 & when\ \varphi' \leq 1 \\ \eta_{su} \approx \frac{1}{\varphi'} & when\ \varphi' > 1 \end{cases} \qquad \text{(Eq. S10)}$$

Table S 3 presents the results obtained for all the catalysts of this study. The minimal values of the Weisz-Prater criterion clearly indicate the absence of internal mass transfer limitations and a surface efficiency close to 1.

Table S 3
Appraisal of possible internal solid mass transfer limitations.

Catalyst	D_{eff} ($m^2.s^{-1}$)	ϕ'	η_{su}
Pd_2	$3.9.10^{-10}$	7.10^{-6}	1
Pd_{10}		2.10^{-5}	1
Pd_{40}		2.10^{-5}	1
Pd_{60}		1.10^{-6}	1
Pd_{200}		4.10^{-6}	1
Pd_{Escat}	$1.1.10^{-10}$	4.10^{-3}	1

S3. Additional data on kinetic experiments and model discrimination

Table S 4

LHHW kinetic rate expressions tested to model AP hydrogenation and PE hydrogenolysis with Pd_{Escat} catalyst.

Entry	Reaction	Hydrogen Activation	Hydrogen adsorption competition	Substrate and products adsorption competition	Limiting step law
1	AP hydrogenation	dissociative	competitive	AP vs. PE	$k_{hydrogenation}\cdot\frac{K_{AC}.C_{AC}(t).\left(K_{H2}.P_{H2}(t)\right)^{0.5}}{(1+K_{AC}.C_{AC}(t)+K_{PE}.C_{PE}(t)+(K_{H2}.P_{H2}(t))^{0.5})^2}$
2		non-dissociative	competitive		$k_{hydrogenation}\cdot\frac{K_{AC}.C_{AC}(t).K_{H2}.P_{H2}(t)}{\left(1+K_{AC}.C_{AC}(t)+K_{PE}.C_{PE}(t).K_{H2}.P_{H2}(t)\right)^2}$
3		dissociative	non-competitive		$k_{hydrogenation}\cdot\frac{K_{AC}.C_{AC}(t)}{1+K_{AC}.C_{AC}(t)+K_{PE}.C_{PE}(t)}.\frac{\left(K_{H2}.P_{H2}(t)\right)^{0.5}}{1+\left(K_{H2}.P_{H2}(t)\right)^{0.5}}$
4		non-dissociative	non-competitive		$k_{hydrogenation}\cdot\frac{K_{AC}.C_{AC}(t)}{1+K_{AC}.C_{AC}(t)+K_{PE}.C_{PE}(t)}.\frac{K_{H2}.P_{H2}(t)}{1+K_{H2}.P_{H2}(t)}$
5	PE hydrogenolysis	dissociative	competitive	AP vs.PE vs. EB vs. water	$k_{hydrogenolysis}\cdot\frac{K_{PE}.C_{PE}(t).(K_{H2}.P_{H2}(t))^{0.5}}{(1+K_{AC}.C_{AC}(t)+K_{PE}.C_{PE}(t)+(K_{EB}+K_{H2O}).C_{EB}(t)+(K_{H2}.P_{H2}(t))^{0.5})^2}$
6		non-dissociative	competitive		$k_{hydrogenolysis}\cdot\frac{K_{PE}.C_{PE}(t).K_{H2}.P_{H2}(t)}{(1+K_{AC}.C_{AC}(t)+K_{PE}.C_{PE}(t)+(K_{EB}+K_{H2O}).C_{EB}(t)+K_{H2}.P_{H2}(t))^2}$
7		dissociative	non-competitive		$k_{hydrogenolysis}\cdot\frac{K_{PE}.C_{PE}(t)}{1+K_{AC}.C_{AC}(t)+K_{PE}.C_{PE}(t)+(K_{EB}+K_{H2O}).C_{EB}(t)}.\frac{\left(K_{H2}.P_{H2}(t)\right)^{0.5}}{1+\left(K_{H2}.P_{H2}(t)\right)^{0.5}}$
8		non-dissociative	non-competitive		$k_{hydrogenolysis}\cdot\frac{K_{PE}.C_{PE}(t)}{1+K_{AC}.C_{AC}(t)+K_{PE}.C_{PE}(t)+(K_{EB}+K_{H2O}).C_{EB}(t)}.\frac{K_{H2}.P_{H2}(t)}{1+K_{H2}.P_{H2}(t)}$

Table S 5

List of experiments used to discriminate and fit the AP hydrogenation and PE hydrogenolysis models using Pd_{Escat}.

Entry	Pressure	Temperature	Initial AP concentration	Initial PE concentration	Initial EB concentration	Initial water concentration	Palladium	Data source	Reactor hydrogen feed type
	(bar)	(°C)	($mol.L^{-1}$)	($mol.L^{-1}$)	($mol.L^{-1}$)	($mol.L^{-1}$)	(mol%)		
1	2	60	0.2	-	-	-	0.2	Hydrogen consumption	constant pressure
2	3	60	0.2	-	-	-	0.2	Hydrogen consumption	constant pressure
3	5	60	0.2	-	-	-	0.2	Hydrogen consumption	constant pressure
4	5	60	0.2	-	-	-	0.2	GC analysis	constant pressure
5	5	44	0.2	-	-	-	0.2	GC analysis	constant pressure
6	5	25	0.2	-	-	-	0.2	GC analysis	constant pressure
7	1	25	0.2	-	-	-	0.2	GC analysis	constant pressure
8	5	60	0.2	0.2	-	-	0.2	GC analysis	constant pressure
9	5	60	0.2	-	0.2	-	0.2	Hydrogen consumption	constant pressure
10	5	60	0.2	-	-	2	0.2	Hydrogen consumption	constant pressure
11	5	60	0.8	-	-	-	0.2	Hydrogen consumption	constant pressure
12	5	60	0.2	-	-	-	0.03	Hydrogen consumption	constant pressure
13	5	60	0.2	-	-	-	0.05	Hydrogen consumption	constant pressure
14	8	60	0.2	-	-	-	0.2	Hydrogen consumption	constant pressure
15	15	60	0.2	-	-	-	0.2	Hydrogen consumption	constant pressure
16	10 → 0	60	0.4	-	-	-	0.2	Hydrogen consumption	closed-batch mode

17	0.3 → 0	60	-	1.6	-	-	0.2	Hydrogen consumption	closed-batch mode

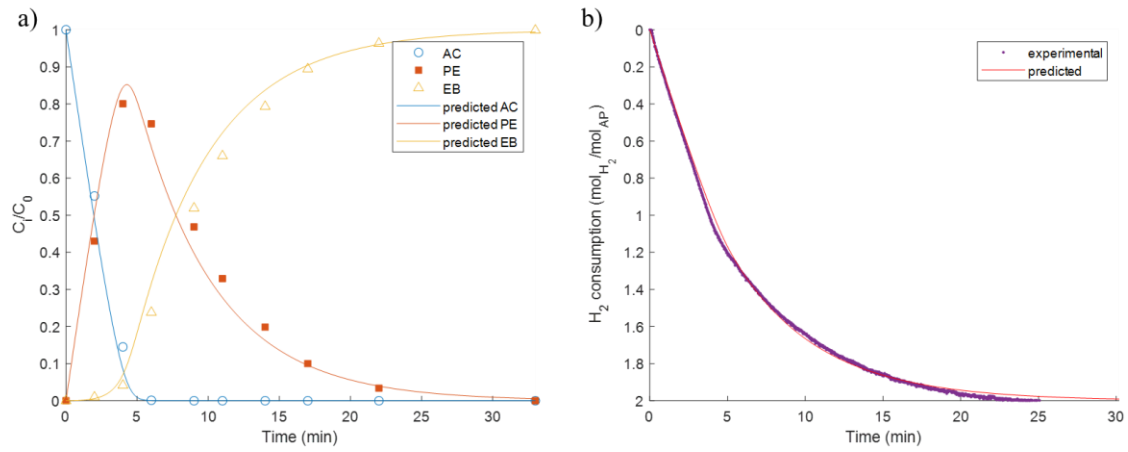

Figure S 4. Typical liquid composition profile and hydrogen consumption profile monitored from reserve during AP reduction using Pd_{Escat} (0.2M AP, 120mL EtOH, 60°C, 5 bar H_2, 0.2mol% Pd). The continuous lines are the responses of the model.

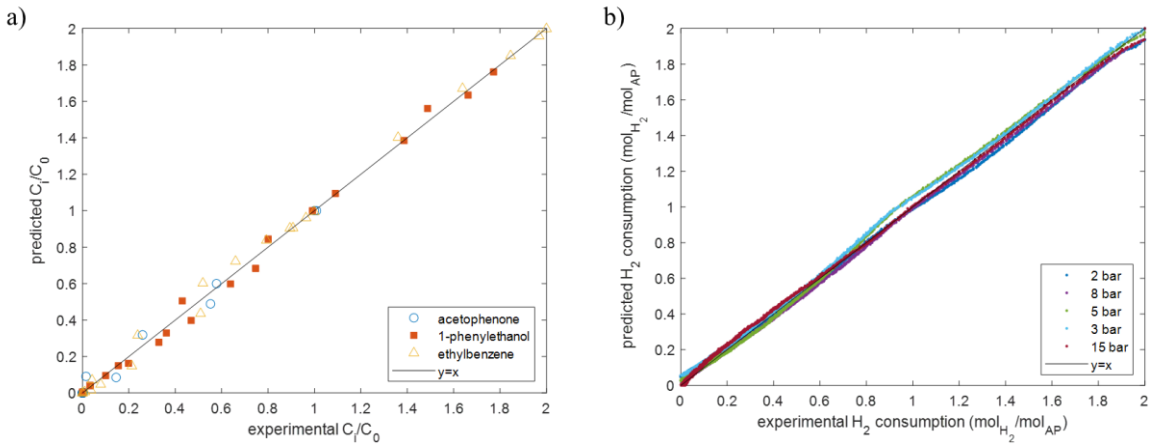

Figure S 5. Parity plots showing a) the experimental composition of the liquid phase vs. predicted concentration and b) experimental consumption of hydrogen vs. predicted consumption of hydrogen during acetophenone reduction with Pd_{Escat} using dissociative and non-competitive models for AP hydrogenation (Table S4 entry 3) and non-dissociative and competitive mode for PE hydrogenolysis (Table S4 entry 6).

Table S 6

Correlation matrix between the regressed adsorption and kinetic parameters with Pd_{Escat} using dissociative and non-competitive models for AP hydrogenation (Table S4 entry 3) and non-dissociative and competitive mode for PE hydrogenolysis (Table S4 entry 6).

	K_{AC} ($L.mol^{-1}$)	K_{PE} ($L.mol^{-1}$)	$K_{EB}+K_{H2O}$ ($L.mol^{-1}$)	K_{H2} (bar^{-1})	$k_{hydrogénation}$ ($mol.h^{-1}.mol_{Pd}^{-1}$)	$k_{hydrogénolyse}$ ($mol.h^{-1}.mol_{Pd}^{-1}$)
Values	139 ± 9	9.0 ± 0.5	9.6 ± 0.6	0.54 ± 0.02	13300 ± 200	34500 ± 800
Correlation matrix	1					
	0.532	1				
	0.656	0.738	1			
	0.595	0.884	0.84	1		
	-0.788	-0.628	-0.83	-0.818	1	
	-0.102	-0.749	-0.14	-0.518	0.09	1

Table S 7

Correlation matrix between the regressed adsorption and kinetic parameters with Pd/CNT series using dissociative and non-competitive models for AP hydrogenation (Table S4 entry 3) and non-dissociative and competitive mode for PE hydrogenolysis (Table S4 entry 6).

	For All Pd/CNT		Pd_{200}		Pd_{60}		Pd_{40}		Pd_{10}		Pd_2	
	K_{PE} (L/mol)	$K_{EB}+K_{H2O}$ (L/mol)	$k_{hydrogenation}$ (mol/h/molPd)	$k_{hydrogenolysis}$ (mol/h/molPd)	$k_{hydrogenation}$ (mol/h/molPd)	$k_{hydrogenolysis}$ (mol/h/molPd)	$k_{hydrogenation}$ (mol/h/molPd)	$k_{hydrogenolysis}$ (mol/h/molPd)	$k_{hydrogenation}$ (mol/h/molPd)	$k_{hydrogenolysis}$ (mol/h/molPd)	$k_{hydrogenation}$ (mol/h/molPd)	$k_{hydrogenolysis}$ (mol/h/molPd)
Values	33 ± 7	75 ± 9	1900 ± 100	1700 ± 200	8000 ± 500	12000 ± 1000	10500 ± 700	32000 ± 3000	14200 ± 900	23000 ± 2000	6400 ± 200	9900 ± 400
Correlation matrix	1											
	0,65	1										
	0,58	0,38	1									
	-0,11	0,10	-0,35	1								
	0,55	0,29	0,32	-0,08	1							
	-0,27	0,46	-0,15	0,22	-0,36	1						
	0,66	0,37	0,38	-0,09	0,37	-0,24	1					
	-0,45	0,27	-0,26	0,21	-0,31	0,74	-0,48	1				
	0,60	0,36	0,35	-0,07	0,34	-0,20	0,40	-0,30	1			
	-0,33	0,42	-0,19	0,22	-0,25	0,78	-0,28	0,76	-0,33	1		
	0,68	0,43	0,39	-0,08	0,38	-0,20	0,45	-0,32	0,41	-0,24	1	
	-0,25	0,43	-0,14	0,20	-0,21	0,72	-0,23	0,69	-0,18	0,73	-0,30	1

S4. References

[1] P.M. Armenante, D.J. Kirwan, Mass transfer to microparticles in agitated systems, Chem. Eng. Sci., 44 (1989) 2781-2796.
[2] E. Dietrich, C. Mathieu, H. Delmas, J. Jenck, Raney-nickel catalyzed hydrogenations: Gas-liquid mass transfer in gas-induced stirred slurry reactors, Chem. Eng. Sci., 47 (1992) 3597-3604.
[3] Z. Junmei, X. Chunjian, Z. Ming, The mechanism model of gas–liquid mass transfer enhancement by fine catalyst particles, Chem. Eng. J., 120 (2006) 149-156.
[4] S. Karve, V.A. Juvekar, Gas absorption into slurries containing fine catalyst particles, Chem. Eng. Sci., 45 (1990) 587-594.
[5] P.B. Weisz, C.D. Prater, Interpretation of Measurements in Experimental Catalysis, in: W.G. Frankenburg, V.I. Komarewsky, E.K. Rideal (Eds.) Advances in Catalysis, Academic Press1954, pp. 143-196.